minerals

MDPI

Article

Methods for Verifying the Relationship Between Weak Uranium Anomaly and Uranium-Rich Geological Bodies in the Covered Areas of the Erlian Basin, Inner Mongolia

Liancheng Shi [1,2], Huaiyuan Li [2,3], Nanping Wang [1,*], Penghui Han [2,3], Zhengxin Shen [2,3], Cong Yu [1], Xiang Zhang [2,3] and Xiangbao Meng [2,3]

[1] School of Geophysics and Information Technology, China University of Geosciences (Beijing), 29 Xueyuan Road, Beijing 100083, China; shiliancheng@briug.cn (L.S.)
[2] Airborne Survey and Remote Sensing Center of Nuclear Industry, 11 Xuefu Road, Shijiazhuang 050002, China
[3] Hebei Key Laboratory of Airborne Survey and Remote Sensing Technology, 11 Xuefu Road, Shijiazhuang 050002, China
* Correspondence: 1996010992@cugb.edu.cn

Abstract

The Erlian Basin, an important research area for sandstone-type uranium deposit exploration in China, is affected by overburden layers, resulting in indistinct characteristics of uranium anomalies in airborne gamma-ray spectrometry (AGS). To harness the potential of AGS, it is imperative to develop effective verification methods that can identify the spatial relationship between weak uranium anomalies and deep uranium-rich geological bodies. This study presents a comprehensive investigation of geophysical and geochemical measurements conducted in four distinct areas. There is a significant positive correlation between the ground gamma spectrometry equivalent uranium (eU_{GGS}) content, soil radon concentration (C_{Rn}), geoelectrochemical uranium (U_{GEC}), and metal activity state uranium (U_{MAS}) content directly above and at the edges of uranium-rich geological bodies. When the buried depth of the uranium-rich geological body exceeds 100 m, the eU_{GGS} content above these deep uranium bodies increases by (0.4–1.2) $\times$ 10^{-6} g/g compared to background areas, while the C_{Rn} levels at the edges of these bodies increase by more than 5000 Bq/m^3, which is 3–5 times higher than the regional average. Meanwhile, the U_{GEC} and U_{MAS} contents show sawtooth-like uranium peak anomalies on their profiles, and their peak-to-background ratio is greater than 5. The verification methods and corresponding interpretation indicators, namely GGS, C_{Rn}, GEC and MAS measurements, can quickly reveal the spatial relationship and provide a reliable basis for concealed uranium deposit exploration.

Keywords: airborne gamma spectrometry; ground gamma spectrometry; soil radon concentration; sandstone type uranium deposit; Erlian Basin

check for updates

Academic Editor: Georgia Pe-Piper

Received: 28 July 2025
Revised: 20 September 2025
Accepted: 21 September 2025
Published: 24 September 2025

Citation: Shi, L.; Li, H.; Wang, N.; Han, P.; Shen, Z.; Yu, C.; Zhang, X.; Meng, X. Methods for Verifying the Relationship Between Weak Uranium Anomaly and Uranium-Rich Geological Bodies in the Covered Areas of the Erlian Basin, Inner Mongolia. *Minerals* **2025**, *15*, 1013. https://doi.org/10.3390/min15101013

Copyright: © 2025 by the authors. Licensee MDPI, Basel, Switzerland. This article is an open access article distributed under the terms and conditions of the Creative Commons Attribution (CC BY) license (https://creativecommons.org/licenses/by/4.0/).

1. Introduction

The Erlian Basin is an important area for sandstone-type uranium deposit exploration in China [1,2]. With the continuous improvement of exploration work, the opportunity to discover near-surface mines is becoming smaller and smaller [3–5]. Compared with the extraction and interpretation of AGS uranium anomalies caused by minerals in bedrock areas, the processing methods of airborne geophysical data in coverage areas are more complex

and the factors to be considered in interpreting this data are more comprehensive [3,4,6]. To further investigate the exploration potential of sandstone-type uranium deposits in this basin, airborne magnetic and AGS measurements were conducted at a scale of 1:50,000, covering an approximate area of 75,000 km^2 from 2018 to 2020 [5,7,8]. Due to the considerable thickness of overlying sedimentary rocks on sandstone-type uranium deposits, often exceeding 100 m [2,5,9], AGS uranium anomalies and direct mineral exploration indicators are not readily discernible, typically presenting as a subtle elevation in eU_{AGS} content [7,8]. This article defines AGS weak uranium anomalies as information affected by surface coverings, where the eU_{AGS} content is less than 3×10^{-6} g/g and the peak-to-background ratio is smaller than 3, yet it shows a slight increase compared to adjacent survey lines and neighboring areas. Weak uranium anomalies can be extracted through techniques such as geological background analysis, data transformation, signal enhancement, and ratio transformation, and it holds certain implications for mineral exploration [3–6,8,10].

Effectively determining the spatial relationship between weak uranium anomalies in basin cover areas and deep uranium-rich geological bodies is crucial for establishing a fundamental basis for sandstone-type uranium exploration. This issue significantly influences the pivotal role of AGS in uranium exploration within basin cover areas.

However, the presence of the thick sedimentary cover above sandstone-type uranium deposits leads to limited surface prospecting information [11,12], thereby constraining the efficacy of conventional radioactive prospecting methods such as geological profile survey, soil geochemical survey, ground gamma total survey, GGS survey, and C_{Rn} measurement [5,9,10,13,14]. Consequently, it becomes challenging to accurately delineate favorable mineralized areas and provide guidance for exploration. Due to the influence of surface sandy soil, clay, sandy gravel layers, etc., there are fewer useful geological phenomena. Abnormal characteristics of K, U, and Th element contents measured by GGS are not obvious, and it is impossible to determine whether a weak increase in local eU content is related to a deep uranium-rich geological body [4]. Differences in total ground gamma radiation measurements are relatively small. Soil geochemical measurements do not show obvious anomalies in shape due to the influence of sampling particle size [15]. C_{Rn} measurements can initially reveal whether there are structural fractures and uranium-rich geological bodies in the lower part of the overburden layer in the abnormal area [4,13,14]. It is a relatively effective method for investigating and verifying anomalies, but it is greatly affected by surface landforms, climate, humidity, etc. [13,14,16–18]. The above methods have significant limitations in identifying the causes of anomalies/weak uranium anomalies and their spatial relationships with deep uranium-rich geological bodies [5,14,17,18]. Therefore, it is urgent to study an effective combination verification method to solve the above-mentioned problems.

In recent years, theoretical and applied research on radon migration, gas transport in the earth, and deep-penetrating geochemistry has shown that deep uranium mineralization can exhibit subtle abnormal information on the surface [5,13,14,17–20]. Therefore, a large number of scholars have conducted deep penetration geochemical measurement experiments [21–31] such as GEC (geoelectrochemical) [5,26–30], MAS (metal activity state) [21,30,31], and geogas [19] on sandstone-type uranium deposits in basins and found that single-element or multi-element anomalies often appear above concealed uranium ore bodies. However, there is little comprehensive research combining the existing verification methods of AGS anomalies and weak uranium anomalies in the basin coverage area [5]. An effective set of combined verification methods and anomaly interpretation models has not yet been formed.

Consequently, the present study has conducted verification work on GGS, C_{Rn}, GEC, and MAS to verify AGS anomalies and weak uranium anomalies in the Hadatu and Barun uranium deposits in the Erlian Basin. We analyze the spatial correlation between uranium-rich geological bodies and various verification parameters by conducting a comparative study of the verification results from four separate study areas. The objective is to identify optimal combinations of verification methods and exploration indicators through comparative analysis of verification outcomes and correlation studies, as well as to establish a model for interpreting anomalies using combined verification methods.

Geological Setting

The Hadatu and Barun uranium deposits in this study are located in the central part of the Erlian Basin [2,12], together with the HFU-34 AGS anomaly and the HFU_R-96 and HFU_R-97 AGS weak uranium anomalies (Figure 1). The study area is located in the Ulanqab and Manite depression, which are in the middle of the Bayinbaolige uplift and Sonid uplift of the Erlian Basin [2,5]. The HFU-34 AGS anomaly is located at the edge of the Naomugen sag in the eastern part of the Ulanqab depression. The Hadatu uranium deposit and the HFU_R-96 and HFU_R-97 AGS weak uranium anomalies are 5 km apart and both are located in the middle of the Qiharigetu sag and east of the Ulanqab depression. The Barun uranium deposit is located in the west of the Tabei sag, which is in the southwest of the Manite depression.

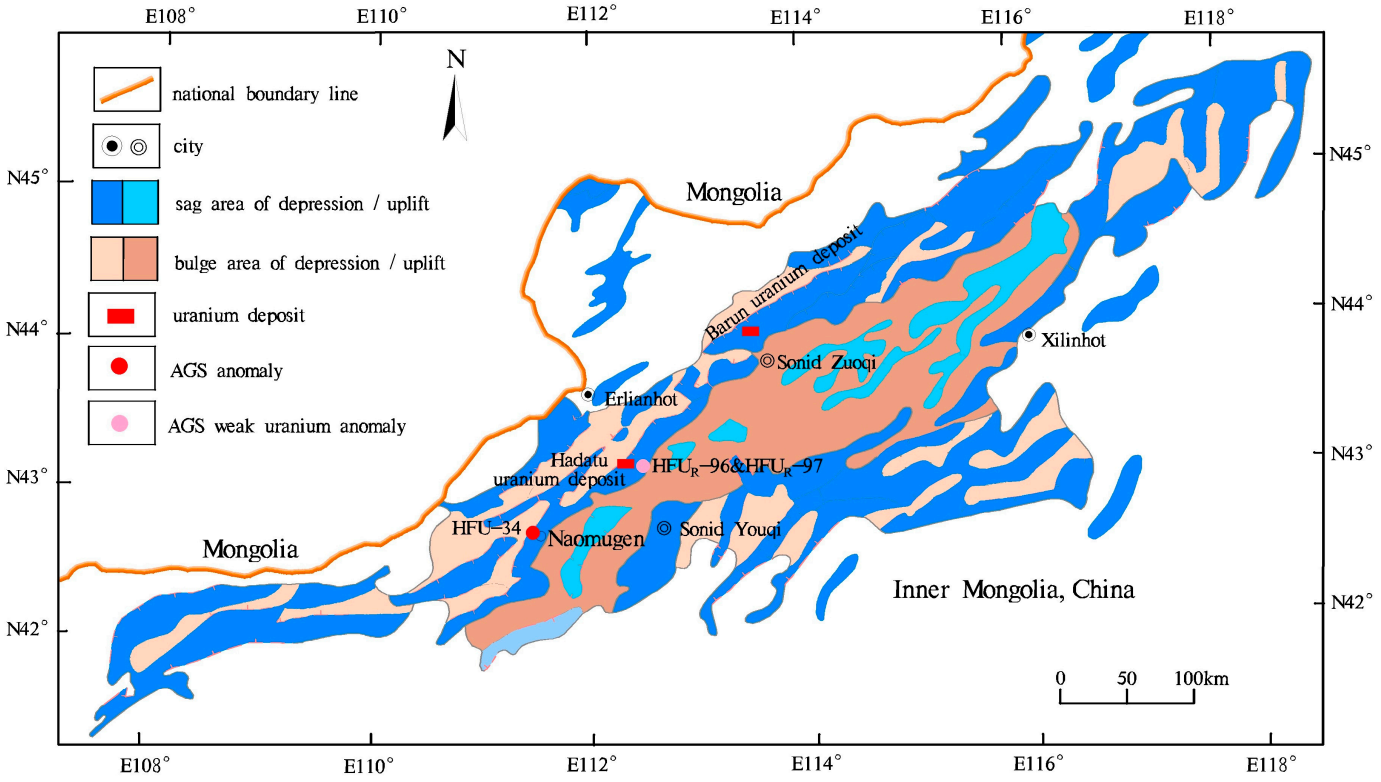


Figure 1. Simplified tectonic geological position map of the study area.

The ore-bearing horizon of the Hadatu and Barun uranium deposits in the study area is the paleo-valley sand body of the upper member of the Saihan Formation, which is obviously controlled by structure and tectonic evolution [2,13,14]. Uranium mineralization has the characteristics of the nearby uranium source. The exposed or hidden medium--acid rock mass around the deposit provides a uranium-rich source for the pre-enrichment and epigenetic mineralization of uranium in the sand body of the ore-bearing horizon [12].

The upper part of the uranium deposit is mainly composed of mudstone and sandstone, with a thin layer of quaternary sandy soil, gravel layers, and vegetation cover on the surface. The depth of burial for the Hadatu uranium deposit ranges from 260 m to 350 m, while the Barun uranium deposit ranges from 90 m to 120 m. In the Naomugen area, uranium mineralization occurs near the surface.

2. Materials and Methods

2.1. Data Collection and Sample Analysis Methods

GGS measurements were conducted using the ARD multi-channel gamma-ray spectrometer produced by the Airborne Survey and Remote Sensing Center of Nuclear Industry (ARCN), Shijiazhuang China. The sampling time was 120 s, and two sets of data were measured at each point. During the measurement process, the probe was placed upright on the ground, and the distance between the probe and the ground was zero. Soil characteristics, gravel composition, gravel content, and vegetation development degree were observed and recorded.

C_{Rn} measurements were conducted using the HDC-C environmental radon detector produced by ARCN, Shijiazhuang, China. The measurements adopted the soil radon model and fixed-point measurements. The soil characteristics, degree of vegetation development, soil compactness, and relative humidity of each measuring point were recorded. The gas sampling depth was 80 cm with a gas volume of 1.5 mL. We completed air extraction 6 to 10 times [5,16]. After completing the air extraction, sampling was carried out for 2 min in powered mode. After sampling ended, the adsorbent carrier was quickly placed in the middle of the gold–silicon surface barrier detector of the radon detector for a 3 min measurement. Three sets of data were measured at each point to obtain an average value.

The GEC measurement included four steps: preparation, burial, retrieval, and testing analysis of the GEC extraction device produced by ARCN, Shijiazhuang, China [26]. In this study, self-developed portable dipole geoelectric extraction instruments were used, along with pole connection devices, high-density polyurethane foam plastic, carbon fiber poles, and non-woven fabric bags to form GEC extraction devices. In the field, the 9 V constant voltage mode was employed with a power supply time of 24 h and a pole distance of 75 cm. The extracting agent used was lemon acid with a concentration of 5%, and each pole required 450 mL of extracting agent. The poles were buried at a depth of 30 cm. The collected samples were subjected to drying, ashing, and digestion processes prior to the analysis of elemental content, including U, Th, Mo, V, and Pb contents, using inductively coupled plasma mass spectrometry (ICP-MS). The detection limits of U, Th, Mo, V, and Pb were 5×10^{-9} g/g, 9×10^{-9} g/g, 80×10^{-9} g/g, 200×10^{-9} g/g, 30×10^{-9} g/g.

The sampling depth for MAS measurement was 10 cm to 30 cm, where fine-grained soil with a −40 mesh size was collected. Prior to laboratory analysis, the samples underwent sieving through a vibrating screen to achieve a −200 mesh size, and the sample weight should not have been less than 50 g. To enhance the representativeness of the samples, combination samples were collected at two to three locations within a range of 2 m at each sampling point. For every 10 g sample, 50 mL of uranium-specific extractant was added and thoroughly mixed. Subsequently, the container was covered and placed in a temperature-controlled oscillator at (25 ± 2) °C for shaking over a period of 4 h, followed by settling for 20 h. After slow filtration using vacuum pressure on filter paper, an 1.0 mL aliquot of the extraction solution was taken and diluted with 3% HNO_3 to reach a final volume of 10 mL for ICP-MS determination [32].

The GEM100P4-95-PLUS-S low-background high-purity germanium (HPGe) gamma spectrometer manufactured by AMETEK ORTEC of Oak Ridge, TN, USA was employed for the measurement of trace amounts of uranium (U_{trace}) and radium (Ra_{trace}). Field samples weighing a minimum of 2 kg were collected, and prior to laboratory testing, soil samples were dried at a constant temperature of 100 °C and crushed through a sieve (40~60 mesh) after extraneous materials were removed, such as weeds and gravel, in accordance with the analytical method. The weighed sample was then placed in a sample box consistent with the standard source of the gamma spectrometer for calibration, sealed, and measured after an incubation period of 25 days.

The AGS data utilized in this study were derived from high-precision airborne geophysical surveys conducted during 2018 and 2019 [5,8]. The data acquisition was performed with a line spacing of 500 m and a flight altitude of 120 m. The RS-500 airborne gamma spectrometer manufactured by Radiation Solutions Inc. of Mississauga, ON, Canadan utilized in the field data collection process comprised 14 NaI (Tl) crystals (14 × 4.2 L). The detector was composed of 12 crystals referred to as the down component of the spectrometer and 2 crystals referred to as the up component of the spectrometer.

2.2. Data Processing Methods

The AGS data was gridized using the minimum curvature method, and an equidistant contour map of eU content was plotted with a grid spacing of 125 m. The profile map of eU content was drawn based on the average value, where the portions above the average were marked in red and those below the average were marked in blue.

The eK_{GGS}, eU_{GGS}, and eTh_{GGS} contents and the C_{Rn} were also processed using the minimum curvature method with a grid spacing equal to one-fourth of the profile line distance.

We performed statistical analyses and calculations to determine the number of measurement points, maximum value, minimum value, average value, median, and standard deviation for the eU_{GGS} content, U_{GEC} content, U_{MAS} content, and C_{Rn} in each research area. Additionally, we generated scatter plots and conducted correlation analyses between different variables to compute the correlation coefficient.

By using statistical methods such as mean (X) and standard deviation (S) combined with a strategy of gradually removing outlier data (i.e., excluding data $\geq X + 2S$ or $\leq X - 2S$), we calculated the background value (X) of C_{Rn} in the measured soil area, as well as the lower limit for outliers (X + 2S). Based on this, values exceeding 5 times the background value (5X) were considered anomalies [17]. Additionally, according to range divisions, when C_{Rn} meets the condition $X + S \leq C_{Rn} \leq X + 2S$, it is defined as slightly elevated; when C_{Rn} meets the condition $X + 2S \leq C_{Rn} \leq X + 3S$, it is defined as elevated; when C_{Rn} meets the condition $X + 3S \leq C_{Rn} \leq 5X$, it is classified as an exceptional anomaly [17].

The calculation formula for the uranium-radium equilibrium coefficient *Kp* can be expressed as follows:

$$K_P = \frac{Ra_{trace}}{U_{trace}} \times \frac{1}{3.4 \times 10^{-7}} \quad (1)$$

where U_{trace} is the trace amount of uranium in the sample; Ra_{trace} is the trace amount of radium in the sample. When $Kp = 1$, it means that the sample is in an equilibrium state with equal amounts of uranium and radium; when $Kp > 1$, it means that the sample has less uranium and more radium; when $Kp < 1$, it means that the sample has more uranium and less radium.

3. Results

3.1. Verification Characteristics of Sandstone-Type Uranium Deposits

According to the principle of known-to-unknown, we conducted GGS, soil C_{Rn}, GEC, and MAS measurements on the Hadatu and Barun uranium deposits in the Erlian Basin. However, data regarding the GGS, soil C_{Rn}, and GEC characteristics of the Hadatu uranium deposit [5], as well as relevant data on the Barun uranium deposit, have been published in other papers [18]. This article focuses on presenting statistical values for various variables of these two known uranium deposits, their correlations with each other, and their comprehensive profile characteristics.

3.1.1. GGS Characteristics of Uranium Deposits

Research has found that the Hadatu uranium deposit study area exhibits a negative correlation between the eU_{GGS} and eTh_{GGS} contents as a whole. Specifically, the main uranium mineralization is associated with a high-value zone in the north–northeast direction and is particularly prominent along the southern margin of the deposit. Additionally, a 'high on both sides and low in the middle' characteristic was observed in the direction perpendicular to the trend of mineralization. The eU_{GGS} content above and around the deposit area is mostly concentrated between (1.73~2.69) $\times 10^{-6}$ g/g, reaching a maximum of 3.35 $\times 10^{-6}$ g/g. However, using the method of calculating the lower limit anomaly by adding three times the standard deviation to the mean value, an anomaly lower limit of 3.5 $\times 10^{-6}$ g/g was obtained, which could not effectively identify uranium mineralization anomalies within the coverage area.

The eU_{GGS} content of the Barun uranium deposit research area exhibits the following characteristics: a slight increase was observed locally above the ore body, while a circular high value was present around the periphery of the ore body. The eU_{GGS} content is mainly concentrated between (1.64~2.46) $\times 10^{-6}$ g/g, with a maximum reaching 2.69 $\times 10^{-6}$ g/g (Table 1). However, using the method of calculating the lower limit anomaly by adding three times the standard deviation to the mean value, an anomaly lower limit of 2.71 $\times 10^{-6}$ g/g was obtained, which could not effectively identify uranium mineralization anomalies within the coverage area.

Table 1. Statistical analysis of verification results for the Hadatu and Barun uranium deposits.

Statistic	Hadatu Uranium Deposit				Barun Uranium Deposit		
	eU_{GGS} (10^{-6} g/g)	C_{Rn} (kBq/m^3)	U_{GEC} (10^{-9} g/g)	U_{MAS} (10^{-9} g/g)	eU_{GGS} (10^{-6} g/g)	C_{Rn} (kBq/m^3)	U_{GEC} (10^{-9} g/g)
Numbers	137	137	134	137	273	281	105
Min value	0.96	1.00	3.58	22.07	0.90	2.50	5.01
Max value	3.35	15.03	105.42	215.00	2.69	91.34	134.87
Average	2.12	4.69	32.69	56.25	1.78	9.90	27.67
Median	2.13	4.39	29.63	48.52	1.75	8.23	24.58
Standard Deviation	0.46	2.74	16.53	29.10	0.31	7.20	17.51

3.1.2. C_{Rn} Characteristics of Uranium Deposits

The C_{Rn} in the research area of the Hadatu uranium deposit primarily exhibits low values above the ore body, with localized weak increases. At the edge of the ore body, a high-value zone emerges, which aligns with both the north–northeast distribution of eU_{GGS} and is indicative of control by north–northeast structures.

The C_{Rn} in the research area of the Barun uranium deposit is characterized by predominantly low values above the ore body, occasionally exhibiting slight increases. A circular high-value zone, consistent with the eU_{GGS} content characteristics, was observed at the periphery of the ore body [18].

3.1.3. Comprehensive Characteristics of Uranium Deposits

On the basis of the comprehensive cross-sections of the Hadatu uranium deposit, as shown in Figure 2a (L1 line) and Figure 2b (L4 line), it can be observed that the eU_{GGS} and C_{Rn} values above the ore body are predominantly low, with localized weak increases of (4–6) kBq/m^3. However, pronounced high values are evident at the edges and periphery of the deposit. The anomalous characteristics of the eU_{GGS} content exhibit limited variations in uranium content, while C_{Rn} displays significant anomalies primarily outside the ore body. According to the comprehensive profile in Figure 2 and Table 1, it can be concluded that the peak-to-background ratio of the eU_{GGS} content is less than 3, with no obvious abnormal features and only weak local increases of (0.5–1.2) $\times$ 10^{-6} g/g. U_{GEC} and U_{MAS} above the uranium deposit demonstrate distinct sawtooth peak anomalies. Nevertheless, the peak-to-background ratio of the U_{GEC} content, at 7.5, compared to the U_{MAS} content, at 4.2, is higher, aligning better with known uranium deposits. In addition to clear peak anomalies in the upper part of the ore body, the U_{MAS} content also presents notable anomalies in areas of uranium mineralization both north and south of the deposit.

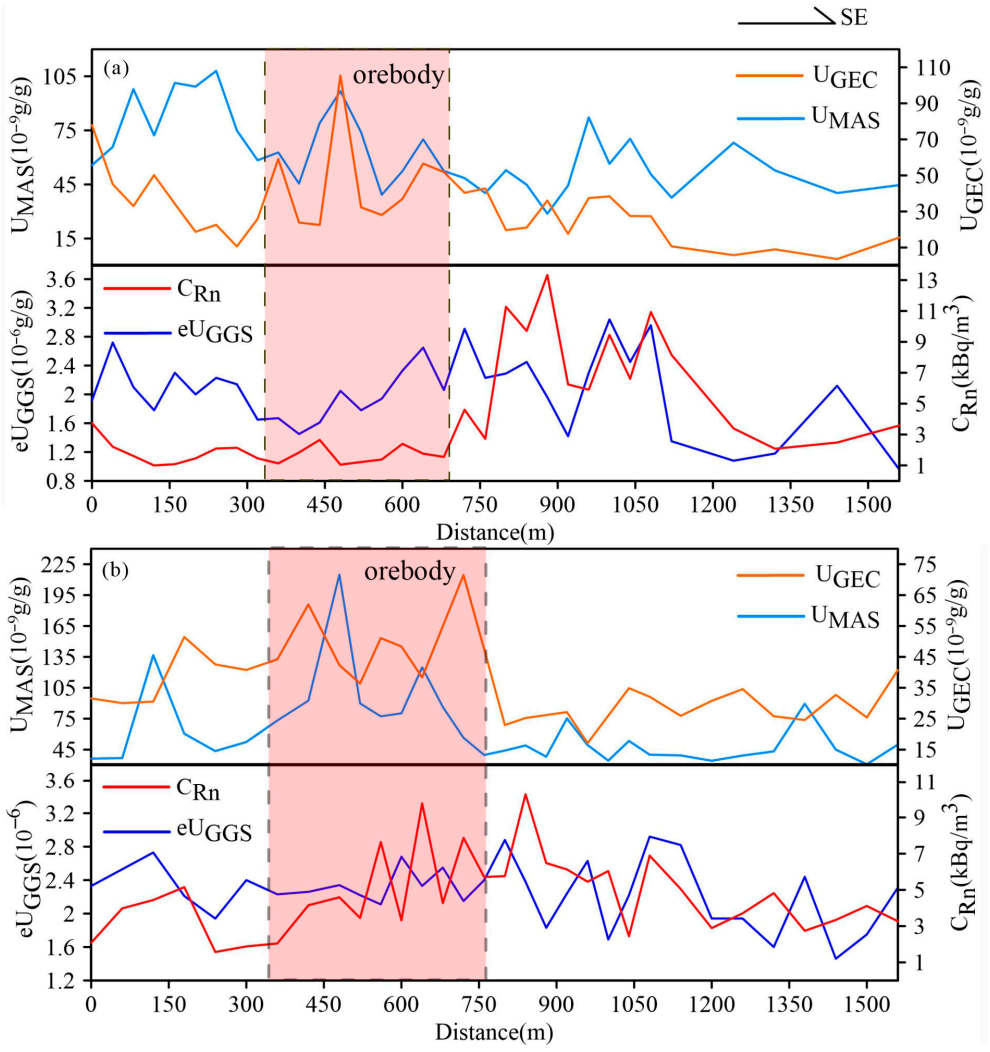


Figure 2. Comprehensive profile map of Hadatu uranium deposit L1 (**a**) and L4 (**b**) line.

As shown in Figure 3, it is evident that the eU_{GGS} and C_{Rn} values above the ore body predominantly exhibit low levels, occasionally showing slight fluctuations, while notable high values can be observed at the edges and periphery of the ore body. The anomalous characteristics of the eU_{GGS} content are not prominently discernible, with minimal variations in the eU_{GGS} content. However, C_{Rn} often displays significant peak anomalies at the periphery of the ore body. Both the U_{GEC} content above the uranium deposit and in the southern mineralized area demonstrate distinct sawtooth-shaped peak anomalies.

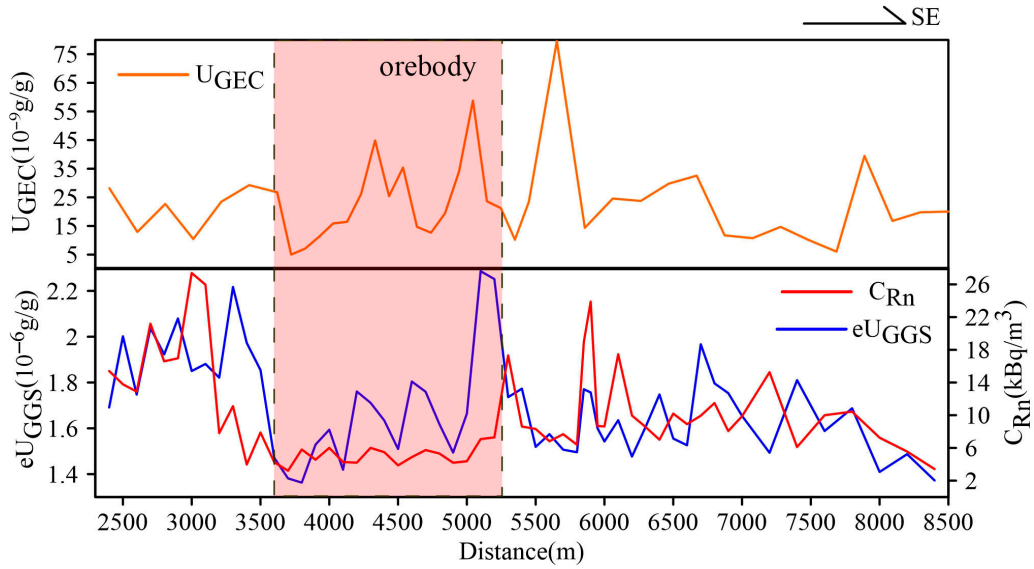


Figure 3. Comprehensive profile map of Barun uranium deposit L1 line.

According to the comprehensive profiles in Figure 3 and Table 1, it can be concluded that the peak-to-background ratio of the eU_{GGS} content is less than 3, with no obvious abnormal features and only weak local increases of (0.4–0.8) $\times 10^{-6}$ g/g. The U_{GEC} content above the uranium deposit demonstrates distinct sawtooth peak anomalies. Nevertheless, the peak-to-background ratio of the U_{GEC} content is 5.2, aligning better with known uranium deposits.

3.2. Verification Characteristics of AGS Anomaly

HFU-34 AGS anomaly was identified at the western edge of the Naomugen sag in the Ulanqab depression, located in the central part of the Erlian Basin. This anomalous area is characterized by a flat terrain and sparse vegetation. A total length of 6.8 km was covered during five GGS and Soil C_{Rn} measurement profiles, with line spacing ranging from 150 m to 200 m and point spacing ranging from 40 m to 80 m. In localized areas, a denser interval of 20 m was used. Additionally, GEC and MAS measurements were conducted on L2 and L4 lines, involving the collection of 50 GEC bubble plastic samples and 35 soil samples for MAS analysis (Figure 4). Furthermore, trace uranium and trace radium analyses were performed on a total of 22 soil and rock samples.

3.2.1. Geological Characteristics of HFU-34 AGS Anomaly

As demonstrated by the regional geological map (Figure 4), the HFU-34 AGS anomaly occurs in various lithologies such as mudstone, siltstone, and conglomerate of the Paleogene Naomugen formation (E_1n). A coeval sedimentary mudstone-type Chagan uranium deposit exists approximately 19 km north of the study area.

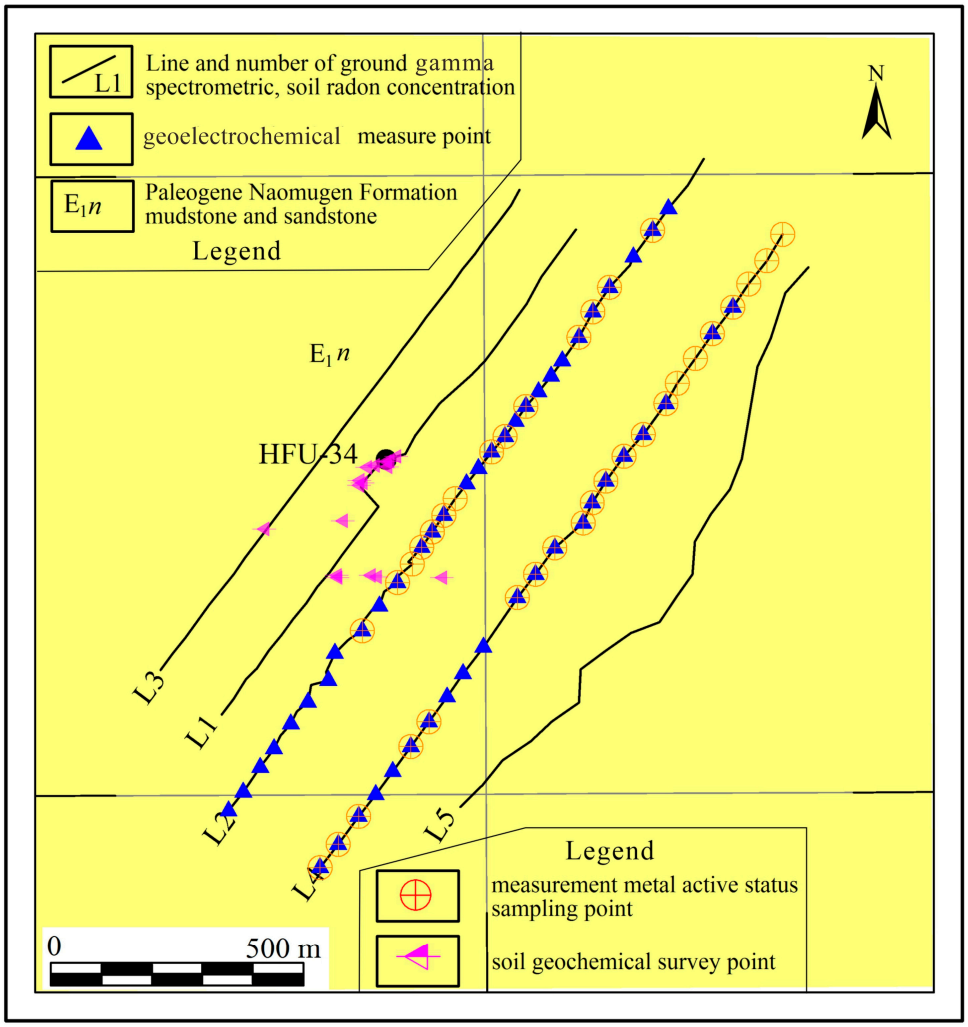


Figure 4. Simplified geological map and actual material map of the HFU-34 AGS anomaly.

Through on-site observation, it was found that the anomalous surface was mainly composed of brown sandy soil and brick-red sandy soil containing a small amount of gravel. In the local area at the center of the anomaly, there were exposed sections of brick-red siltstone and mudstone (Figure 5a,b) of the Paleogene Naomugen formation (E_1n), as well as gray-white, gray-green, and gray-black mudstone. In addition, there were also a few ferritization mudstone nodules (Figure 5c) and siltstone present, with sporadic occurrences of ferritization and secondary uranium minerals (Figure 5d) in the gray-green and gray-black mudstone (Figure 5d). The development characteristics of different-colored mudstone and silty mudstone indicated that this area had undergone changes in redox environments, providing favorable geochemical barriers for uranium migration enrichment. No obvious fault structures were observed, and from a topographic perspective, this anomaly was located in a transitional zone between bulges and sags.

3.2.2. AGS Characteristics of HFU-34 AGS Anomaly

Based on the plane profile (Figure 6a) and contour map (Figure 6b) of the eU content of the HFU-34 AGS anomaly, we could observe a clear peak anomaly phenomenon, with one traverse line showing significant variations while the two lines on both sides displayed weak responses. This anomaly had an equiaxial shape, with a peak value of eU reaching 6.0×10^{-6} g/g and a half peak width of approximately 224 m. In comparison, the eK and eTh contents did not exhibit obvious anomalies, with the eK content at 1.5% and eTh content at 6.4×10^{-6} g/g. Meanwhile, the eU/eTh ratio was calculated as 0.94.

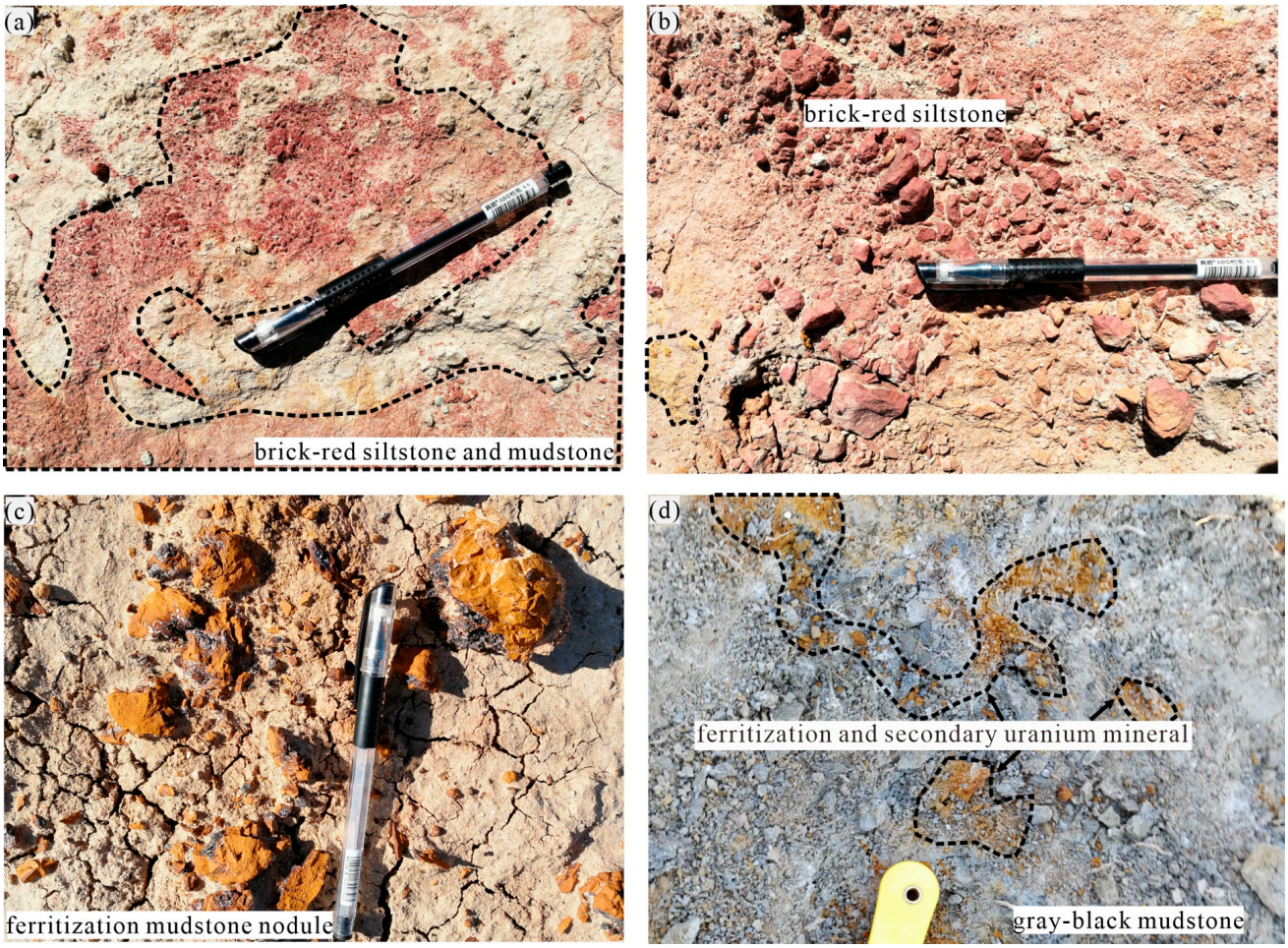


Figure 5. Surface geological phenomena of HFU-34 AGS anomaly. (**a**) brick-red siltstone and mudstone, (**b**) brick-red siltstone, (**c**) ferritization mudstone nodule, (**d**) ferritization and secondary uranium mineral.

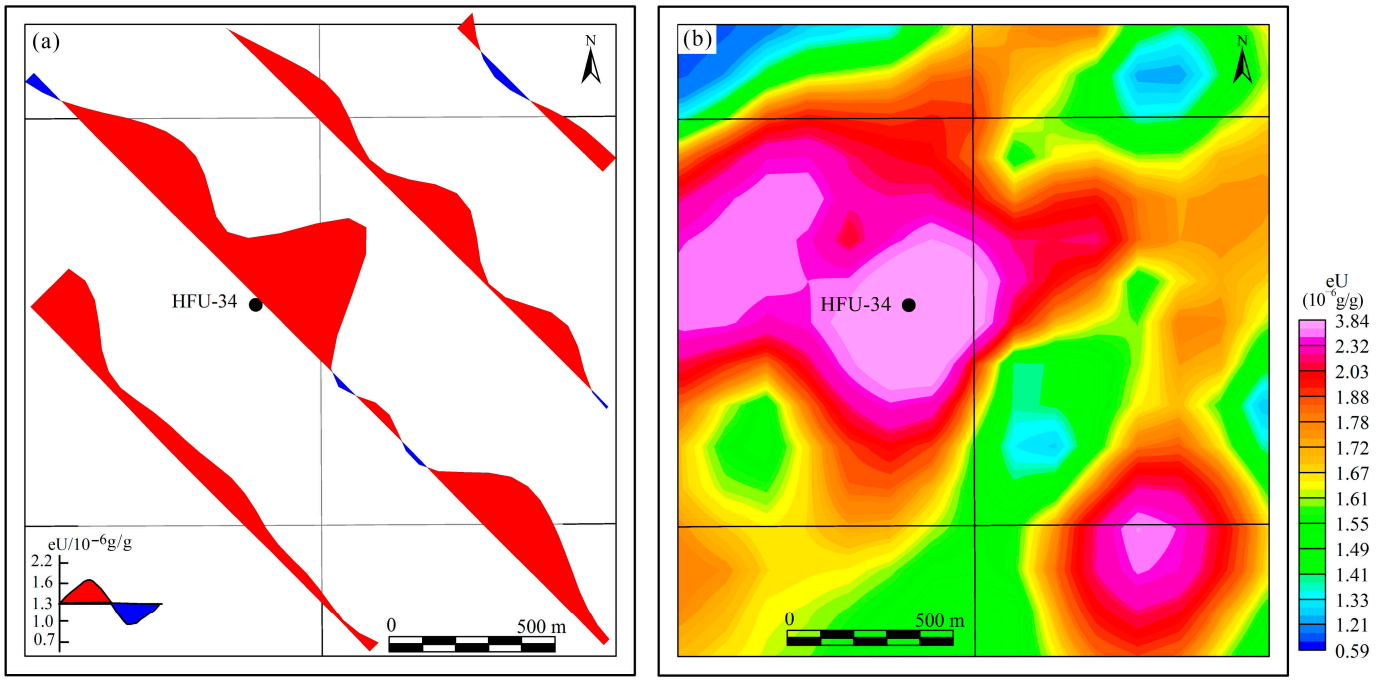


Figure 6. Plane profile (**a**) and contour map (**b**) of AGS eU content of HFU-34 AGS anomaly.

3.2.3. GGS Characteristics of HFU-34 AGS Anomaly

Based on the contour map of the eU_{GGS} content (Figure 7b), it can be observed that the U anomaly and its surrounding high values exhibit an axisymmetric distribution from the north-east to near the east-west. The range of the anomaly was approximately 180 m, while the radius of eU_{GGS} high-value points was about 50 m. A total of 147 data sets were collected, with eU_{GGS} content ranging from a minimum of 1.61 × 10^{-6} g/g to a maximum of 158.6 × 10^{-6} g/g, with an average value of 5.23 × 10^{-6} g/g and a median value of 3.25 × 10^{-6} g/g. These data conform to the characteristics of a positively skewed distribution (Table 2).

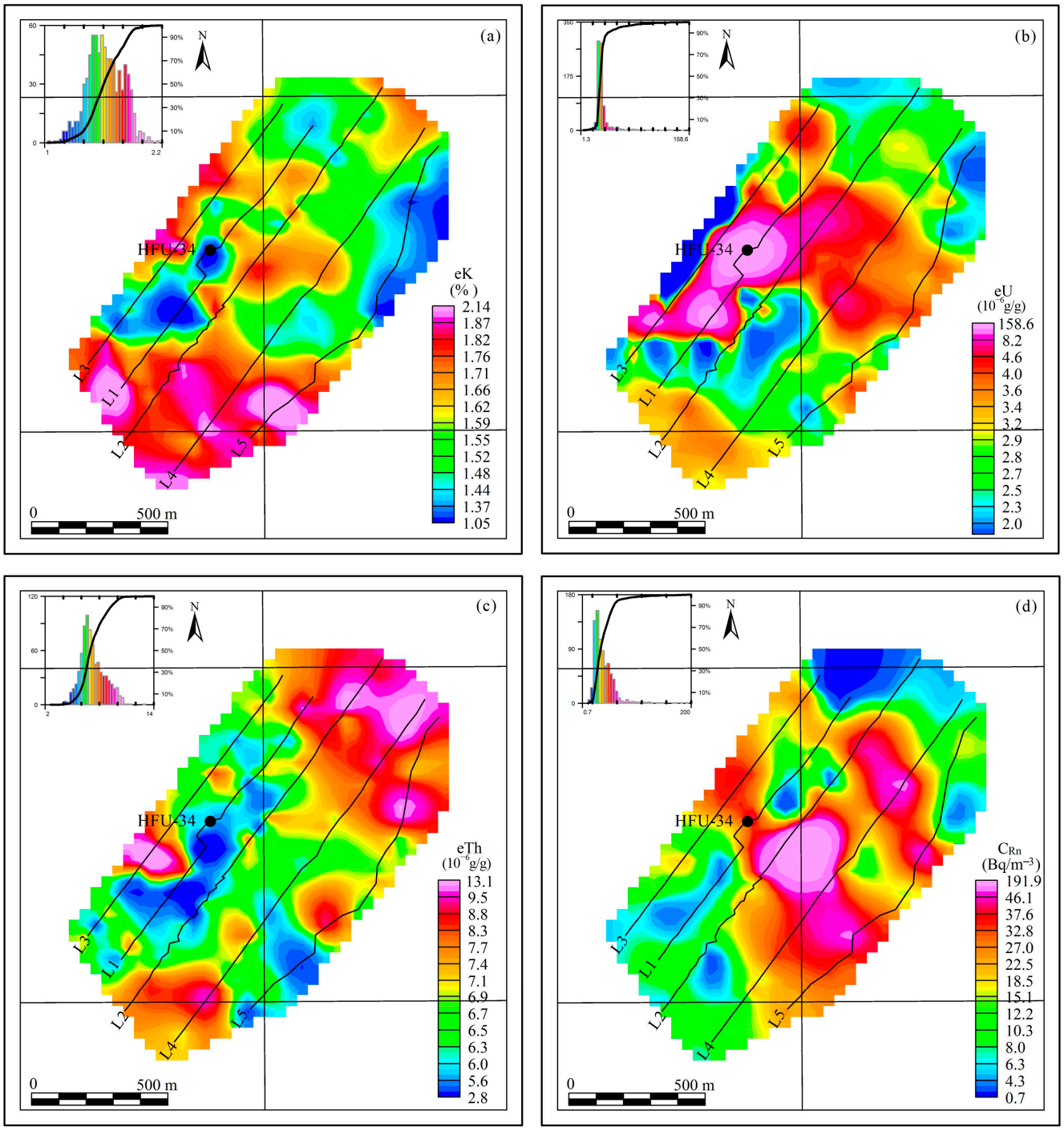


Figure 7. Contour map of GGS eK (**a**), eU (**b**), eTh (**c**) contents and C_{Rn} (**d**) of HFU-34 AGS anomaly.

Table 2. Statistical analysis of verification results for HFU-34 AGS anomaly.

Statistic	eU_{GGS} (10^{-6} g/g)	C_{Rn} (kBq/m^3)	U_{GEC} (10^{-6} g/g)	U_{MAS} (10^{-9} g/g)	U_{trace} (10^{-9} g/g)	Ra_{trace} (10^{-9} g/g)	K_p
Numbers	147	148	50	35	22	22	22
Min value	1.61	1.33	18.70	48.38	4.25	14.25	0.99
Max value	158.6	220.25	275.91	478.93	1878.16	6291.82	0.99
Average	5.23	21.27	81.24	184.72	178.84	599.11	0.99
Median	3.25	15.56	48.56	97.37	28.52	95.54	0.99
Standard Deviation	7.42	18.34	51.84	107.28	427.66	1432.62	-

The eU_{GGS} content of the HFU-34 AGS anomaly generally ranged from (5.07~10.14) $\times 10^{-6}$ g/g, with a maximum of up to 158.6 $\times 10^{-6}$ g/g, and the average of the anomaly's eU_{GGS} content was 8.85 $\times 10^{-6}$ g/g. The background eU_{GGS} content was (1.56~3.25) $\times 10^{-6}$ g/g, and the average of the background eU_{GGS} content was 2.56 $\times 10^{-6}$ g/g. In the weathered gray-green mudstone, beneath a thin layer of sand soil about 80 m northeast of the anomaly center, the eU_{GGS} content reached as high as 10.1 $\times 10^{-4}$ g/g, and a small amount of secondary uranium minerals were observed to be present. Figure 7a,c show that there was no significant abnormal variation in the eK_{GGS} and eTh_{GGS} contents, with the eK_{GGS} content mainly distributed between 1.44% and 1.71%, reaching a maximum of up to 2.14%. However, the eTh_{GGS} content was distributed in block-like patterns in the western and northern regions of the anomaly center within a range of (8.0~10.1) $\times 10^{-6}$ g/g, with a maximum of up to 13.1 $\times 10^{-6}$ g/g.

3.2.4. C_{Rn} Characteristics of HFU-34 AGS Anomaly

Table 2 shows that a total of 148 C_{Rn} data were collected. Among them, the minimum value was 1.33 kBq/m^3, the maximum was 220.25 kBq/m^3, the average value was 21.27 kBq/m^3, and the median was 15.56 kBq/m^3. These data exhibit a positively skewed distribution (Figure 7d). By gradually excluding abnormal data, the background value (X) for this anomalous C_{Rn} was determined to be 13.6 kBq/m^3 with a standard deviation (S) of 7.3 kBq/m^3. Additionally, the lower limit (X + 2S) for anomalies was set at 28.3 kBq/m^3 (Table 3).

Table 3. Statistical analysis of C_{Rn} verification results for HFU-34 AGS anomaly (kBq/m^3).

Parameters	X	S	X + S	X + 2S	X + 3S	5X
Value	13.6	7.3	20.9	28.3	35.5	68

According to the contour map of C_{Rn} (Figure 7d), the anomaly exhibits an approximately parallel northwest-oriented band-like distribution, indicating a possible merging of deep anomalies into a larger anomalous area. Additionally, multiple small anomalous halos were developed on the western side of the anomaly band. At a distance of approximately 150 m east from the center of the anomaly, the C_{Rn} reached its maximum at 220.25 kBq/m^3, with the surface covered by brown sandy soil.

As shown in Figure 7b, the anomalous and high-value areas of the eU_{GGS} content are mainly distributed between L3 and L2 survey lines. In this area, the soil cover is relatively thin and locally exposed with gray-white, gray-green, and brick-red mudstone, siltstone, and sandy mudstone. The abnormal C_{Rn} in the soil and its surrounding halo are mainly located in the sandy soil-covered area to the east of line L2 (Figure 7d). Due to poor sampling effectiveness in areas where bedrock is exposed and differences in buried depth of uranium-rich mudstone, there is inconsistency between the spatial distribution of radon concentration in soil and the anomalous areas of eU_{GGS} content.

Based on comprehensive analysis of surface geological features, GGS characteristics, and C_{Rn} characteristics in the research area, we believe that a uranium-rich geological body has developed deep underground, leading to abnormal C_{Rn} and a surrounding anomalous halo.

3.2.5. Comprehensive Characteristics of HFU-34 AGS Anomaly

As shown in the comprehensive profiles of the L2 and L4 lines of the HFU-34 AGS anomaly in Figure 8, there are obvious peak anomalies in the eU_{GGS} content, C_{Rn}, U_{GEC} content, and U_{MAS} content. These peak anomaly sections coincide with each other. During the field data collection process, as the sampling depth increased, the values of C_{Rn} anomaly sections rapidly rose. Meanwhile, in the L2 line profile, the C_{Rn} reached 220.25 kBq/m^3 compared to a background value of 13.6 kBq/m^3, with a peak-to-background ratio of 16.2. Therefore, it can be concluded that this anomaly was caused by deep mineralization rather than structural or other factors.

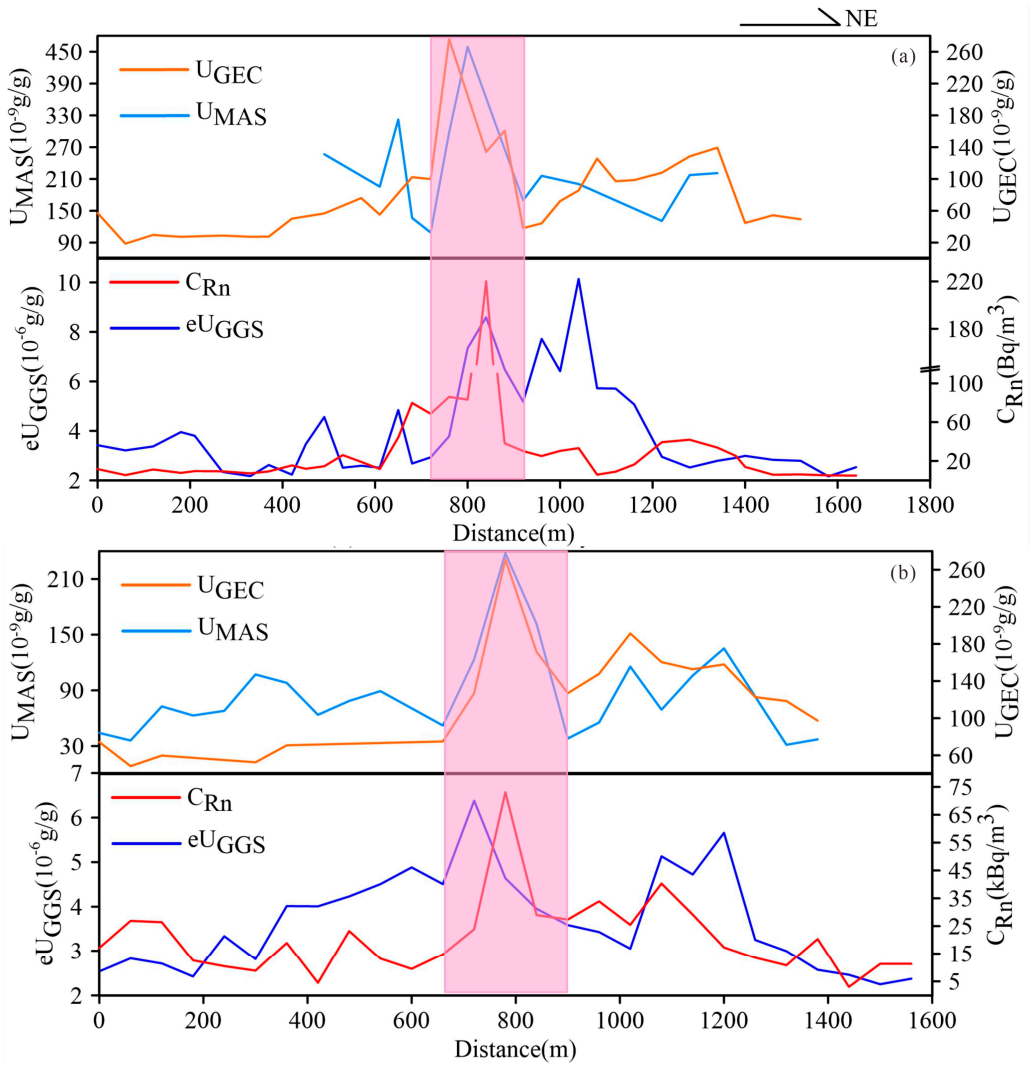


Figure 8. Comprehensive profile map of the HFU-34 AGS anomaly L2 (**a**) and L4 (**b**) line.

At a distance of (920–1100) m from the L2 line, there is an abnormal peak in the eU_{GGS} content (Figure 8). However, there are no anomalies in the C_{Rn}, U_{GEC} content, and U_{MAS} content. This suggests that the elevated surface uranium content in the region is a result of localized enrichment of uranium within the surface materials, rather than the emergence of deep-seated uranium mineralization or enriched uranium geological formations. The

measurement results indicate that, at a distance of 1000–1300 m along the L4 line, there is a weak peak anomaly in the C_{Rn}, U_{GEC} content, and U_{MAS} content. From this, it can be inferred that the potential uranium geological body in this area may have a greater burial depth or a relatively low uranium content.

In addition, K, U, Th, and Ra analysis tests were conducted on the samples collected from the L2 line, as shown in Figure 4, and its western region. The U_{trace} content in the hematite muddy concretion was 0.015%, while the highest U_{trace} content in the gray-black and gray-green mudstone at the center of the anomaly area was 0.196%. Four samples had U_{trace} contents exceeding 0.0293%, while other samples mostly ranged from (19~78) $\times 10^{-6}$ g/g, with U-Ra equilibrium coefficients (Kp) all less than 1 (Table 2), indicating uranium enrichment characteristics. According to sample analysis results, there was a strong enrichment of uranium elements at an industrial level in local shallow-covered or near-surface areas of the anomaly zone. Meanwhile, both AGS and GGS showed overall high eU and low eTh characteristics.

3.3. Verification Characteristics of AGS Weak Uranium Anomaly

Based on the characteristics of sandstone-type uranium mineralization in the Hadatu deposit and the 1:50,000 AGS data from 2019, two weak uranium anomalies were successfully identified: HFU_R-96 and HFU_R-97. These anomalies are located within the Qiharigetu sag of the Ulanqab depression in the middle of Erlian Basin, approximately 65 km away from Sonid Youqi. The region has a flat terrain with sparse vegetation. Three southwest–northeast and two northwest–southeast GGS and C_{Rn} measurement profiles were established. Specifically, for the southwest–northeast profiles, line spacing was set at 130 m with point intervals ranging between (40–60) m, while denser sampling at intervals of (20–30) m were conducted in anomalous areas. The length of the five profiles was 7.38 km. The northwest–southeast profiles passed through two weak uranium anomalies that exhibited abnormal C_{Rn} perpendicular to high-value zones. Point intervals were set at (40–60) m with a profile length of 2 km. Additionally, 31 soil geochemical samples were collected. Furthermore, MAS and GEC measurements were carried out along Line L1, with 42 GEC foam plastic samples and MAS soil samples collected (Figure 9).

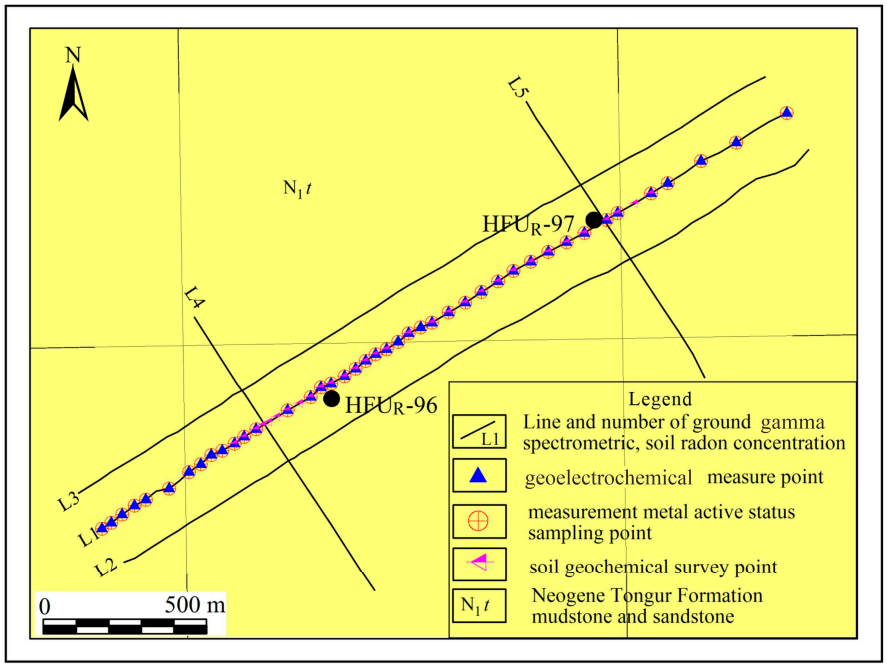


Figure 9. Simplified geological map and actual material map of the HFU_R-96 and HFU_R-97 weak uranium anomalies.

3.3.1. Geological Characteristics of HFU_R-96 and HFU_R-97

As shown in Figure 9, the study area of HFU_R-96 and HFU_R-97 is located in the Neogene Tunggur Formation (N_1t). The Tunggur Formation (N_1t) mainly consists of mudstone, sandstone, and conglomerate. The Hadatu uranium deposit was discovered in the underlying Cretaceous sandstone about 5 km west of the research area. Through field observations, we found that the surface of this area was mainly sandy brown soil, which contained gravel with different particle sizes and degrees of variation. The composition of gravel was complex, featuring sub-angular or sub-rounded shapes, with a primary particle size ranging from 0.5 cm to 2.2 cm. Considering the peripheral stratigraphic characteristics and regional geological data, it was speculated that conglomerate, coarse sandstone, fine sandstone, and mudstone exist in the lower part of this research area.

3.3.2. AGS Characteristics of HFU_R-96 and HFU_R-97

According to the profile plots of the eU content in AGS measurements for HFU_R-96 and HFU_R-97 shown in Figure 10a, it can be observed that the peak value of the eU content for HFU_R-96 is 2.36×10^{-6} g/g, while for HFU_R-97, it is 1.81×10^{-6} g/g. The four measurement lines show a slight increasing trend. As shown in the contour map of the AGS eU content for HFU_R-96 and HFU_R-97 (Figure 10b), it is broadly characterized by a cluster extending from east to west and a weakly elevated zone stretching towards the northeast. Considering the oxidized–reduced transition zone surrounding the Hadatu uranium deposit in the western part of the study area, profiles deployed in both the northwest and northeast directions were verified through multiple ground-based methods.

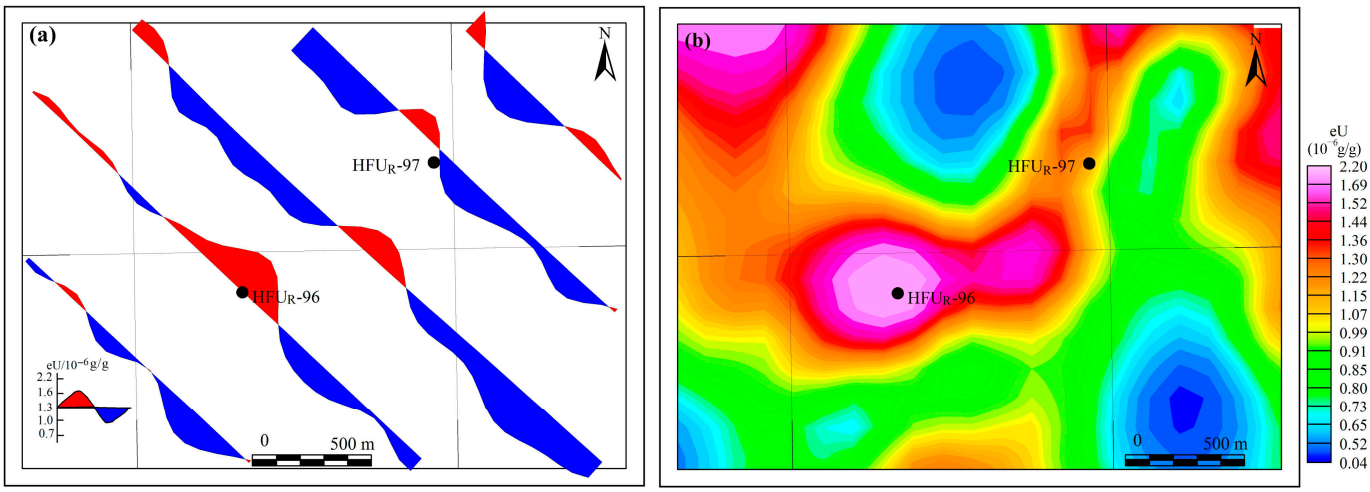


Figure 10. Plane profile (**a**) and contour map (**b**) of AGS eU content of HFU_R-96 and HFU_R-97.

3.3.3. GGS Characteristics of HFU_R-96 and HFU_R-97

According to Figure 11a, the anomalous features of the eK_{GGS} content are not obvious. Overall, it shows a weak elevation band sandwiched between HFU_R-96 and HFU_R-97, with localized high-value clusters corresponding to areas with higher gravel content on the surface. The background value of the eK_{GGS} content ranges from 1.65% to 2.29%, while the high values range from 2.46% to 2.60%.

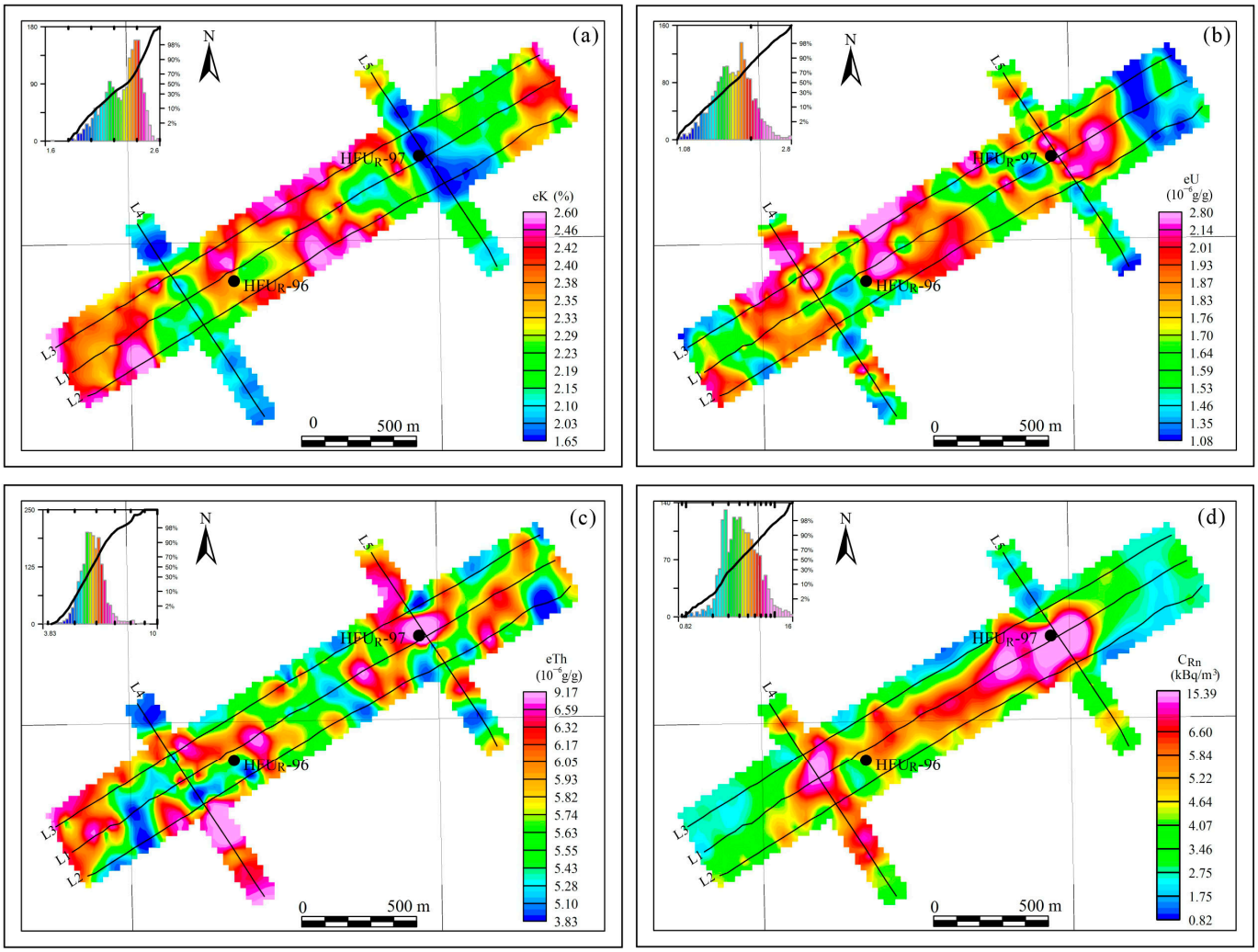


Figure 11. Contour map of GGS eK (**a**), eU (**b**), and eTh (**c**) contents and C_{Rn} (**d**) of HFU$_R$-96 and HFU$_R$-97.

The eU_{GGS} content is distributed in multiple block-like high-value clusters in a northeast direction, as depicted in Figure 11b. Additionally, a weakly elevated zone exhibits a northwest distribution. In the western part of the study area, the weakly elevated uranium zone has an approximate width of 300 m, while it measures about 500 m in the central part and around 300 m in the eastern part. The radius of high-value clusters superimposed on this weakly elevated uranium zone mostly falls within the range of (50–100) m. Analyses based on Figure 11b and Table 4 reveal that the eU_{GGS} content ranges from a minimum of 1.07×10^{-6} g/g to a maximum of 2.83×10^{-6} g/g, with an average of approximately 1.76×10^{-6} g/g and a median close to 1.73×10^{-6} g/g, following a normal distribution pattern consistently observed across various samples analyzed within this study area. Moreover, background values for the eU_{GGS} content range between (1.07–1.73) $\times 10^{-6}$ g/g, while higher values are found within (2.3–2.83) $\times 10^{-6}$ g/g.

Based on Figure 11c, it is evident that the eTh_{GGS} anomalous distribution primarily manifests in the northern and southern perimeters of the centers of HFU$_R$-96 and HFU$_R$-97, with a radius predominantly ranging from 50 m to 80 m. This corresponds to the region with lower sand and gravel content and slightly increased clay content on the surface. The background values of the eTh_{GGS} content range between (3.83–5.74) $\times 10^{-6}$ g/g, while the anomalous values fall within the range of (7.63–9.17) $\times 10^{-6}$ g/g.

Table 4. Statistical analysis of verification results for HFU_R-96 and HFU_R-97.

Statistic	eU_{GGS} (10^{-6} g/g)	C_{Rn} (kBq/m^3)	U_{GEC} (10^{-6} g/g)	U_{MAS} (10^{-9} g/g)	U_{trace} (10^{-9} g/g)	Ra_{trace} (10^{-9} g/g)	K_p
Numbers	204	203	42	42	31	31	31
Min value	1.07	0.78	14.12	20.72	1.35	4.76	0.79
Max value	2.83	15.77	82.38	135.34	3.87	12.14	1.16
Average	1.76	4.80	29.73	51.59	2.20	7.04	0.95
Median	1.73	4.01	17.60	30.77	2.12	6.49	0.92
Standard Deviation	0.36	2.60	11.66	24.76	0.61	1.89	0.11

3.3.4. C_{Rn} Characteristics of HFU_R-96 and HFU_R-97

According to Table 4, a total of 204 sets of actual collected data on C_{Rn} were recorded. The minimum and maximum values observed were 0.78 kBq/m^3 and 15.77 kBq/m^3, respectively, with an average value of 4.80 kBq/m^3 and a median value of 4.01 kBq/m^3. These values exhibit a normal distribution. By iteratively eliminating aberrant data points, the background value for C_{Rn} was determined to be 3.31 kBq/m^3, accompanied by a standard deviation of 0.77 kBq/m^3 and a lower threshold for abnormalities of 4.85 kBq/m^3 (refer to Table 5).

Table 5. Statistical analysis of C_{Rn} verification results for HFU_R-96 and HFU_R-97 (kBq/m^3).

Parameters	X	S	X + S	X + 2S	X + 3S	5X
Value	3.31	0.77	4.08	4.85	5.61	16.56

From the contour map of C_{Rn} (Figure 11d), it can be observed that the C_{Rn} exhibits a cluster-like anomaly halo with "two highs and one low" in a northeast direction, as well as an elevated halo in a northwest direction. The radius of the anomalous halo indicated by HFU_R-97 is approximately 200 m, with a maximum of 15.77 kBq/m^3. On the other hand, HFU_R-96 shows that the radius of the anomalous halo for C_{Rn} is about 80 m, with a maximum of 10.06 kBq/m^3. Above these areas with anomalous C_{Rn} halos, there is mainly a distribution brown sandy topsoil containing small amounts of gravel and clay.

The abnormal C_{Rn} in the study area is consistent with the high eU_{GGS} content. Combining the surface geological features and GGS and C_{Rn} characteristics of the study area, it can be inferred that there are north-eastward and north-westward fracture distributions and deep-seated uranium-rich geological bodies.

3.3.5. Comprehensive Characteristics of HFU_R-96 and HFU_R-97

According to the comprehensive profiles in Figure 12 and Table 4, it can be concluded that the peak-to-background ratio of the eU_{GGS} content is less than 3, with no obvious abnormal features and only weak local increases. The C_{Rn} exhibits a peak anomaly pattern characterized by "two highs and one low", while both the U_{GEC} content and U_{MAS} content show peak anomalies. Furthermore, all three of them have peak-to-background ratios greater than 4, which effectively distinguishes between background values and anomalies.

The peak anomalies of C_{Rn} at the distance of (400–700) m correspond to areas exhibiting slightly elevated U_{MAS} content, increased U_{trace} content in the soil, enriched uranium regions with $Kp < 1$, reduced eU_{GGS} content, and diminished clay content on the ground. The peak anomalies of C_{Rn} at the distance of (1700–2100) m correspond to areas exhibiting slightly elevated U_{MAS} content, higher U_{trace} content in the soil, enriched radium regions with $Kp > 1$, higher eU_{GGS} content, and relatively higher gray-green clay content on the ground. The two regions that previously displayed anomalous spikes in C_{Rn} did not exhibit corresponding peaks in U_{GEC} content. Through comprehensive analysis, it was concluded

that uranium particles and their radioactive isotopes were transported upwards along fault structures from deep underground and locally concentrated through adsorption on surface clay minerals, which are situated at a certain distance from concealed geological formations rich in uranium.

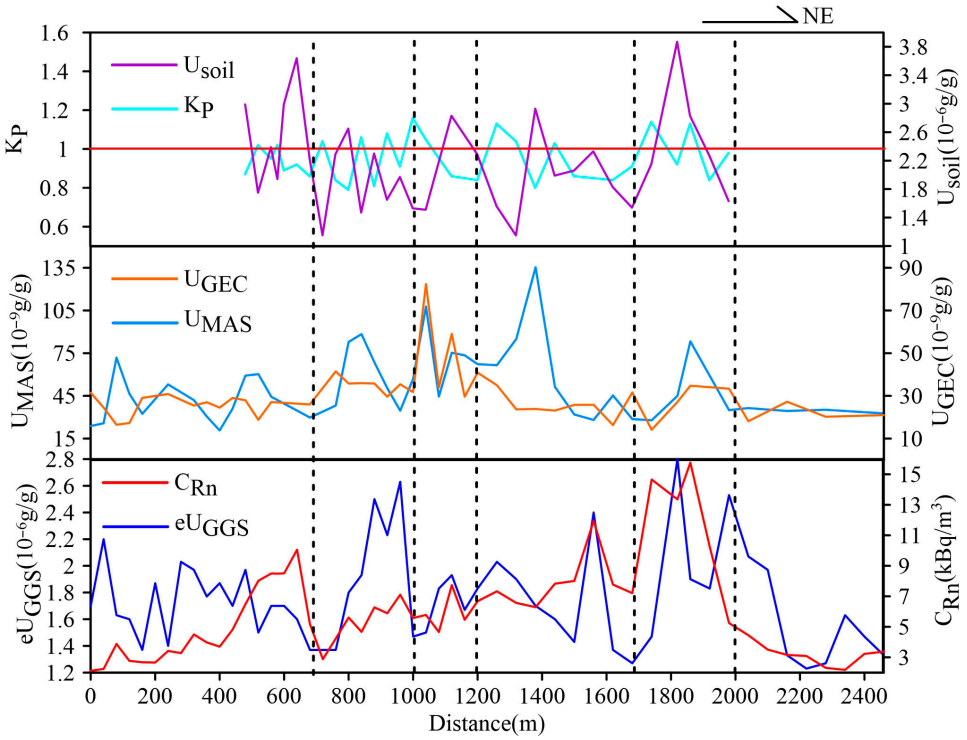


Figure 12. Comprehensive profile map of the HFUR-96 and HFUR-97 L1 line.

The high-value area of the eU_{GGS} content at the distance of (700–1000) m corresponds to the weak peak anomaly zone of the U_{MAS} content and enriched uranium regions with Kp < 1. However, there are no abnormal displays in C_{Rn}, U_{trace}, and U_{GEC} content. The eU_{GGS} content shows a slight increase at distances of (1000–1200) m with (0.8–1.2) × 10^{-6} g/g and (1200–1500) m with (0.9–1.3) × 10^{-6} g/g. The C_{Rn} shows a slight increase at distances of (1000–1200) m with (2–3) kBq/m^3 and (1200–1500) m with (2.8–5.7) kBq/m^3. The U_{MAS} content shows a peak anomaly, trace uranium shows high values, and the uranium–radium equilibrium coefficient Kp < 1 indicates enriched uranium characteristics. In addition, both electrochemical and metal-active uranium exhibit sawtooth-shaped peak anomalies at a distance of (1000–1200) m with good consistency; furthermore, weak peak anomalies were observed in soil radon concentration and ground gamma spectrum U content at a distance of (1500–1600) m.

In summary, the eU_{GGS} content and C_{Rn} in the weak uranium anomalies research area mainly showed low values, with slight increases observed locally. At the same time, there was a peak anomaly in the U_{MAS} content and U_{GEC} content. This combination of anomalies is consistent with those above the Hadatu and Barun uranium deposits. Therefore, it is believed that these areas with combined anomalies have significant mineral exploration potential.

4. Discussion

4.1. Comparison and Analysis of Verification Results

The ore body of the Barun uranium deposit is controlled by ancient river channel sand bodies and is distributed in a layered-plate-like pattern, with relatively good overall continuity. The main ore body, which is currently controlled, extends intermittently for

about 1400 m, with a width ranging from 75 to 900 m and an average thickness of 7.19 m. The thickest part is located in the southwest section, gradually thinning towards the north and east–west sides, with an average grade of 0.02% U and a burial depth of 90 to 110 m.

The ore body of the Hadatu uranium deposit is characterized by a burial depth of 200 to 450 m, an extension of 12 km, a width of 100 to 800 m, and multiple layers of plate-like and lens-shaped structures, with an average grade of 0.06% U. The ore body is strictly controlled by ancient river valleys, fault structures, and post-formation gray sand bodies, meeting the scale and grade conditions for in situ leaching mining. The corresponding uranium ore body in the study area has a burial depth of 300 to 360 m.

According to Tables 6 and 7, the Pearson correlation coefficients calculated based on eU_{GGS}, C_{Rn}, U_{GEC}, and U_{MAS} data indicate a weak overall correlation among these four variables in relation to the Hadatu and Burun sandstone-type uranium deposits, AGS uranium anomalies, and weak uranium anomalies. Specifically, there was a positive correlation between the eU_{GGS} content and C_{Rn}, with correlation coefficients of 0.09, 0.14, 0.16, and 0.23. Additionally, there was also a positive correlation between the eU_{GGS} and U_{MAS} contents, with correlation coefficients of 0.19, 0.25, and 0.04. Furthermore, it was found that there is a positive correlation between the U_{GEC} and U_{MAS} contents, with correlation coefficients of 0.20, 0.32, and 0.41.

Table 6. Pearson correlation matrix of the verification results for sandstone-type uranium deposits.

	Hadatu Uranium Deposit					**Barun Uranium Deposit**		
	eU_{GGS}	C_{Rn}	U_{GEC}	U_{MAS}		eU_{GGS}	C_{Rn}	U_{GEC}
eU_{GGS}	1				eU_{GGS}	1		
C_{Rn}	0.09	1			C_{Rn}	0.14	1	
U_{GEC}	0.18	−0.05	1		U_{GEC}	−0.13	−0.05	1
U_{MAS}	0.19	−0.12	0.20	1				

Table 7. Pearson correlation matrix of the verification results for AGS anomaly and weak uranium anomalies.

	HFU-34					**HFU_R-96 and HFU_R-97**			
	eU_{GGS}	C_{Rn}	U_{GEC}	U_{MAS}		eU_{GGS}	C_{Rn}	U_{GEC}	U_{MAS}
eU_{GGS}	1				eU_{GGS}	1			
C_{Rn}	0.16	1			C_{Rn}	0.23	1		
U_{GEC}	0.23	0.41	1		U_{GEC}	0.10	0.01	1	
U_{MAS}	0.25	0.14	0.32	1	U_{MAS}	0.04	0.15	0.41	1

Based on the analysis results of Figures 2, 13 and 14 and Table 6, these findings suggest that, within the entire uranium deposit research area, the variable data exhibits a discrete nature with limited correlation. However, at the uppermost and peripheral positions of the uranium ore body, these variables demonstrate a distinct positive correlation relationship with an appropriate degree of spatial deviation (Figure 2). This feature suggests that, for the intricate mineralization process of sandstone-type uranium deposits, mere bivariate statistical analysis is insufficient. Instead, a comprehensive approach that employs multiple methods and variables for both profile and plane analysis is more beneficial for identifying favorable exploration zones. The peak values of C_{Rn}, U_{GEC}, and U_{MAS} in the sandstone-type uranium deposit research area predominantly correspond to regions exhibiting a slightly elevated eU_{GGS} content compared to the background value. The C_{Rn} and eU_{GGS} content above the sandstone-type uranium ore bodies predominantly exhibit low levels, with

localized weak increases, while notable high values are observed at edges and periphery of the ore body. This feature differs from radon and progenitor migration to the surface, as it is influenced by the development of dense mudstone in the upper part of the sandstone-type uranium deposit, the discontinuity of the mudstone layer at the boundary and adjacent area of the deposit, the large porosity and uneven pore structure of the sandstone, groundwater flow, and fracture structure, among other factors. The U_{GEC} and U_{MAS} within the ore bodies display peak anomalies. Conversely, outside the deposit, there are often peak anomalies in C_{Rn}, accompanied by slight elevations in U_{GEC}, U_{MAS}, and eU_{GGS} content. This pertains to the regulation of ancient river valleys and faults in the Hadatu and Barun sandstone-type uranium deposits, aligning with the principle that uranium particles and radon progeny can migrate to the surface through faults under various influences.

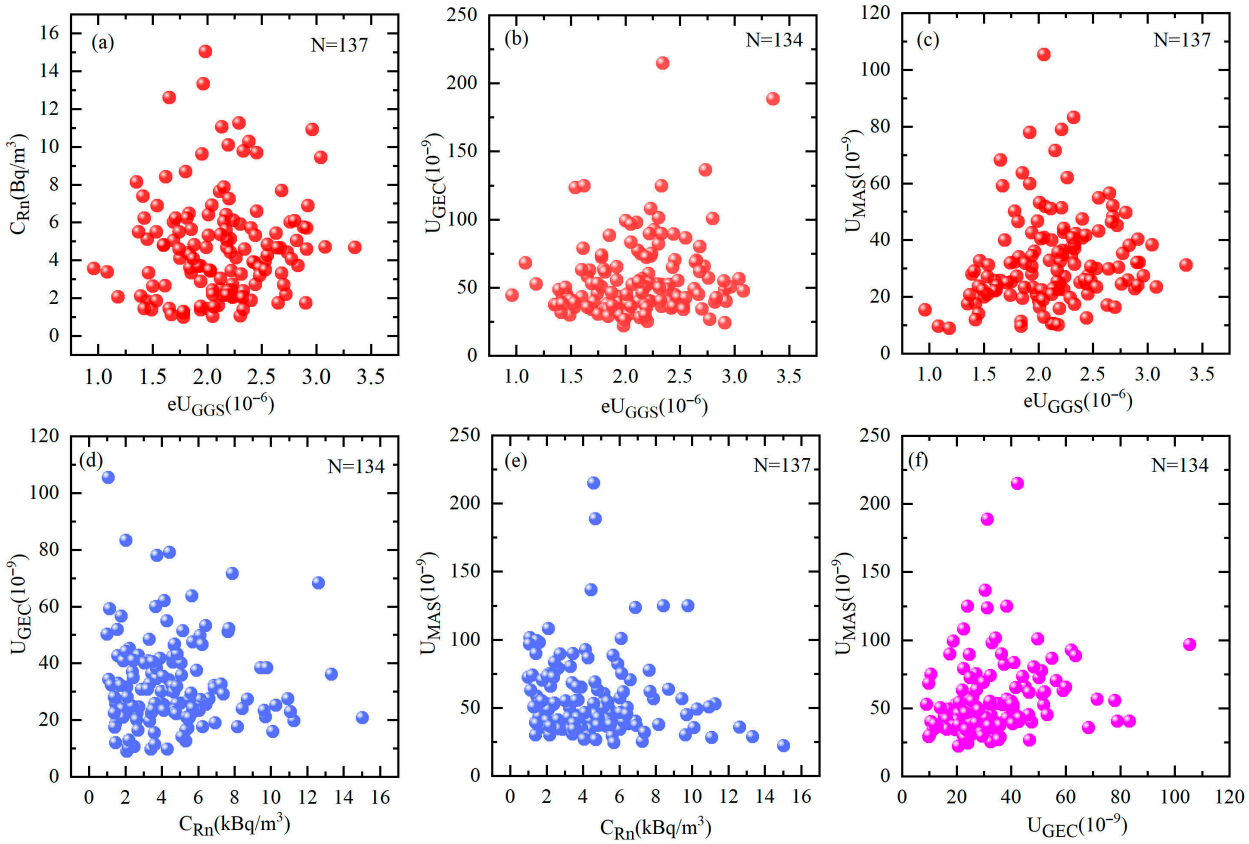


Figure 13. Scatter plots (**a**) eU_{GGS} vs. C_{Rn}, (**b**) eU_{GGS} vs. U_{GEC}, (**c**) eU_{GGS} vs. U_{MAS}, (**d**) C_{Rn} vs. U_{GEC}, (**e**) C_{Rn} vs. U_{MAS}, (**f**) U_{GEC} vs. U_{MAS} of the Hadatu uranium deposit.

After conducting an investigation, it was determined that the HFU-34 anomaly, characterized by shallow uranium mineralization and burial depth, exhibited significant peak anomalies in eU_{GGS} content, C_{Rn}, U_{GEC} content, and U_{MAS} content. These four variables demonstrated a positive correlation in areas where uranium deposits and mineralization occurred. Figure 15 illustrates that the peak values of C_{Rn}, U_{GEC}, and U_{MAS} within the HFU-34 anomaly area mostly corresponded to regions slightly above the background values of the eU_{GGS} content. This finding aligns with verification results from the Hadatu and Barun uranium deposits. By combining Figures 7 and 15 with surface geological observations, it can be demonstrated that the peak anomalies of eU_{GGS} content do not necessarily indicate deep-seated enriched uranium geological bodies. For instance, Figure 7 along Line L2 at a distance of (900–1100) m on the comprehensive profile line exhibits a peak anomaly in eU_{GGS} content, while C_{Rn}, U_{GEC}, and U_{MAS} only show weak increases. A comprehensive analysis suggests that this particular peak anomaly in the eU_{GGS} content is caused by active

uranium adsorbed by surface clay and cannot effectively indicate deep-seated enriched uranium geological bodies in this region.

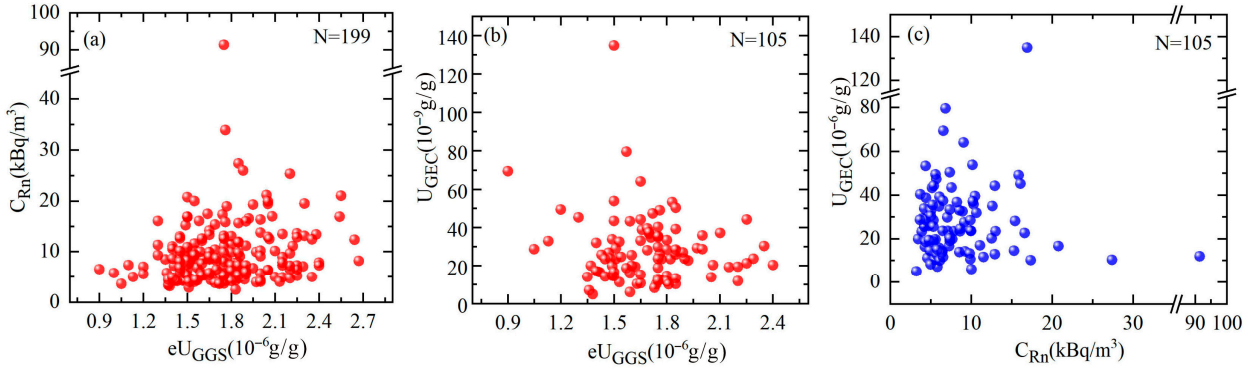


Figure 14. Scatter plots (**a**) eU_{GGS} vs. C_{Rn}, (**b**) eU_{GGS} vs. U_{GEC}, (**c**) $C_{Rn\ vs.}$ U_{GEC} of the Barun uranium deposit.

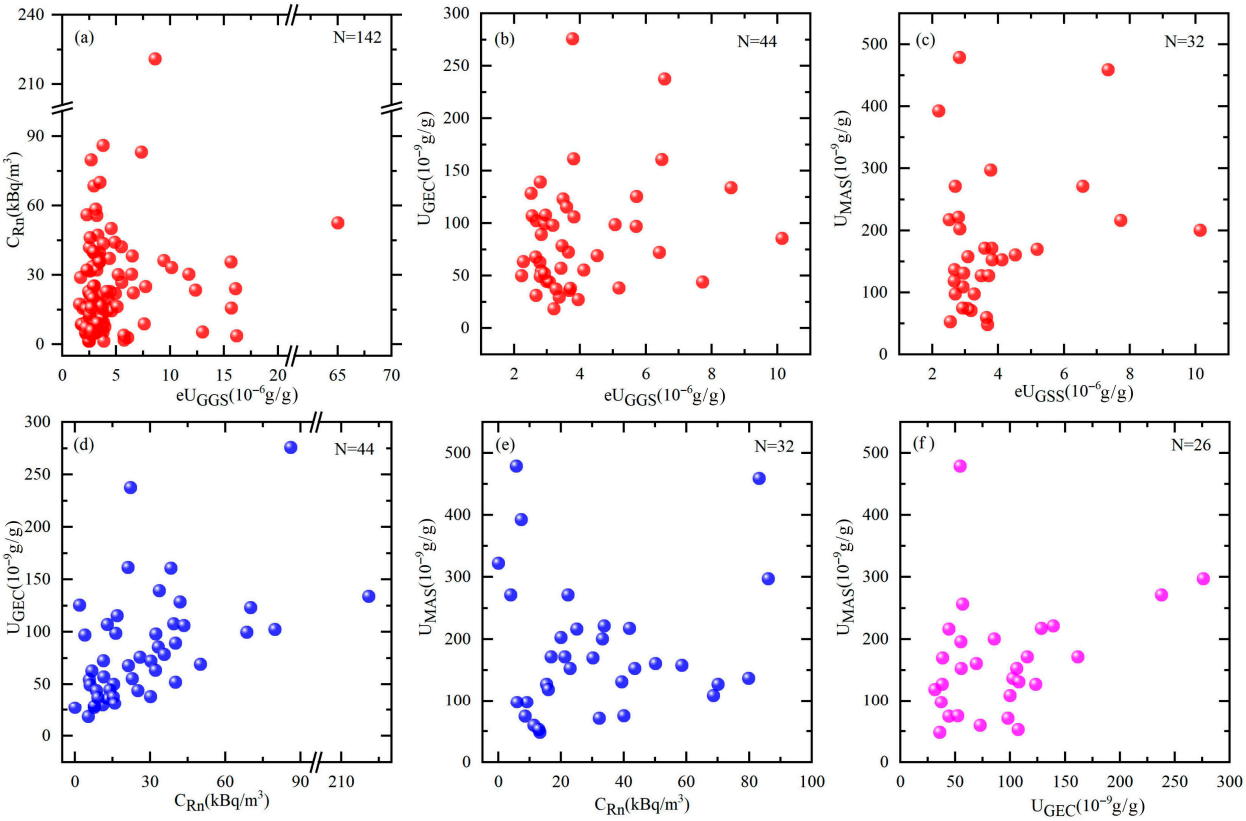


Figure 15. Scatter plots (**a**) eU_{GGS} vs. C_{Rn}, (**b**) eU_{GGS} vs. U_{GEC}, (**c**) eU_{GGS} vs. U_{MAS}, (**d**) $C_{Rn\ vs.}$ U_{GEC}, (**e**) $C_{Rn\ vs.}$ U_{MAS}, (**f**) U_{GEC} vs. U_{MAS} of the HFU-34 AGS anomaly.

According to the results of Table 7 and Figure 16, there is a low correlation among the four variables investigated in the weak uranium anomalies research area, and the data shows a scattered distribution. However, positive correlations were observed between the eU_{GGS} content and C_{Rn} as well as two sets of variables related to the U_{GEC} and U_{MAS} contents. Figure 16 illustrates that the peak values of C_{Rn}, U_{GEC}, and U_{MAS} within the area mostly corresponded to regions slightly above the background values of eU_{GGS} content. This finding aligns with verification results from sandstone-type uranium deposits and the HFU-34 anomaly. According to comprehensive research based on surface geological observations and verification results, it is believed that the weak increases in the U_{GEC} and

U_{MAS} contents corresponding to a weak peak in C_{Rn} and high eU_{GGS} content may have been caused by the adsorption of active uranium by surface or near-surface clay. The weak increase in the U_{GEC} and U_{MAS} contents corresponding to abnormal C_{Rn} may have been due to the migration of active uranium or radioactive substances along fault structures within deep uranium-rich geological bodies.

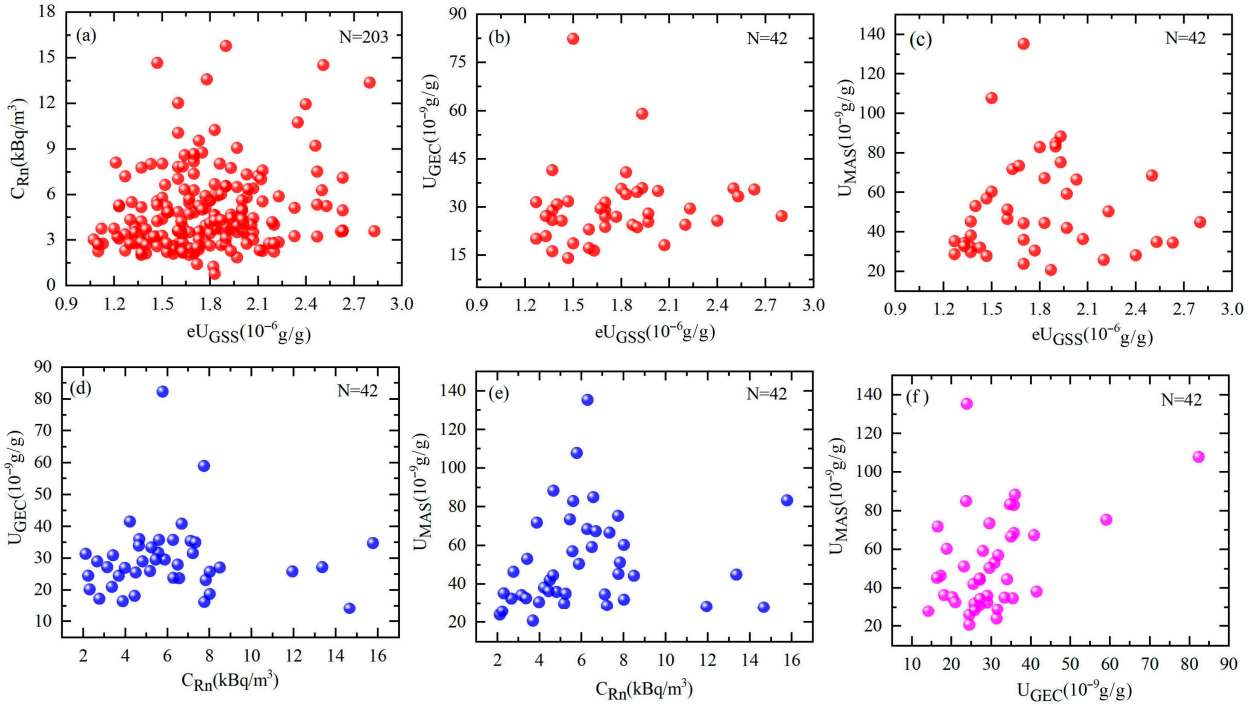


Figure 16. Scatter plots (**a**) eU_{GGS} vs. C_{Rn}, (**b**) eU_{GGS} vs. U_{GEC}, (**c**) eU_{GGS} vs. U_{MAS}, (**d**) C_{Rn} vs. U_{GEC}, (**e**) C_{Rn} vs. U_{MAS}, (**f**) U_{GEC} vs. U_{MAS} of HFU_R-96 and HFU_R-97.

In summary, investigating the spatial coupling and correlation among the four variables can serve as a foundation for comprehending the underlying factors responsible for AGS weak uranium anomalies and their spatial association with uranium-rich geological formations.

4.2. Identification of Effective Verification Methods

Through the above research and discussion, we believe that detailed observation of surface cover types, material composition and content, humidity, fracture structure, and vegetation conditions play an important role in the analysis of C_{Rn} and eU_{GGS}, U_{GEC}, and U_{MAS} content anomaly characteristics in later stages. However, during the verification process of AGS weak uranium anomalies in covered areas, it is not possible to fully utilize the advantages of geological observations in exposed bedrock areas to directly discover fractured zones, altered mineralization, and stratigraphic contact boundaries.

The results obtained from GGS measurements primarily reflect the contents of eK, eU, and eTh in surface coverings rather than those in deep mineral deposits and strata [3–6]. However, after comprehensive evaluation of the application effects in the four study areas, it was found that this method could effectively identify differences in uranium content in surface coverings and reveal slight increases displayed by GGS above deep uranium deposits. As a conventional approach for radioactive measurement, it remains essential to adhere to this method for verification purposes during future coverage area investigations.

The measurement of C_{Rn} was conducted to determine the concentration of radon and its progeny within a depth range of 80 cm below the surface. Due to their strong migration ability along fault structures, radon and its progeny are prone to form high-value

or anomalous zones on the ground [10,14,17–20]. Influenced by sedimentary materials such as mudstone overlying sandstone-type uranium deposits, the C_{Rn} above deep-seated uranium deposits mainly exhibit localized weak increases with relatively low values. In combination with the spatial distribution patterns of sandstone-type uranium deposits and fault structures, this method can be used as an indirect means to reveal the spatial relationship and genetic relationship between AGS weak uranium anomalies and deep-seated uranium geological bodies, but it has certain limitations in directly revealing deep-seated uranium mineralization.

By integrating previous studies and applied research conducted in the known sandstone uranium deposit study area [5,22,24–28], it is postulated that U_{GEC} and U_{MAS} content exhibit peak anomalies above the uranium ore body in profiles and high-value areas, accompanied by localized anomalies on a plane. Moreover, when the depth of burial of the uranium ore body is significant, peak anomalies in U_{GEC} and U_{MAS} content correspond to low-value areas with locally weak increases in eU_{GGS} content and C_{Rn}. Conversely, for shallowly buried uranium ore bodies, there exists a strong spatial correlation between peak anomalies identified through these four verification methods. Henceforth, measurement techniques such as GEC and MAS should be considered more effective in elucidating information pertaining to deeply seated enriched geological formations of uranium.

The eU_{GGS} was calculated by integrating the in situ gamma-ray intensity of radionuclide ^{238}U and its progeny in surface media with the uranium-radium balance coefficient to ascertain the equivalent uranium content. U_{MAS} and U_{GEC} refer to the elemental mass fractions obtained from laboratory chemical analyses of samples, such as rocks, soils, and adsorbent carriers. Although these two methods theoretically exhibit a linear positive correlation under ideal conditions, significant discrepancies often arise in practical applications. Notably, strong correlations are frequently observed in areas characterized by intense uranium mineralization and well-developed ore bodies. GGS offers rapid and cost-effective detection with sensitivity to the radioactive uranium–radium balance in shallow media. MAS and GEC geochemical surveys provide accurate data that represent true ore concentrations, serving as essential references for evaluating deep mineralization. High U_{MAS} or U_{GEC} contents with low eU_{GGS} content may indicate downward enrichment of uranium, meriting consideration for deep prospecting. Conversely, high eU_{GGS} content accompanied by low U_{MAS} or U_{GEC} contents typically suggests surface-level uranium enrichment or potassium–thorium interference, necessitating cautious interpretation.

Based on the verification results and correlation analysis of multiple methods in four research areas, as well as a comprehensive study on the effectiveness and limitations of various methods in revealing deep uranium mineralization information, we believe that two combined methods based on surface geological observations can effectively determine the spatial and genetic relationship between anomalies or weak information and deep uranium-rich geological bodies. One method is to combine GGS, C_{Rn}, and GEC measurements. The other method is to combine GGS, C_{Rn}, and MAS measurements. These methods provide a basis for exploration of concealed uranium deposits.

4.3. Construction of a Model for Identifying Mining Signs and Their Interpretation

After conducting comprehensive research and analysis, a clear positive correlation was observed between the eU_{GGS} content, C_{Rn}, U_{GEC} content, and U_{MAS} content above and around uranium-rich geological bodies. In cases where the depth of uranium-rich geological bodies was significant, localized weakly increased low values were predominantly observed in the eU_{GGS} content and C_{Rn}. These observations corresponded to sawtooth peak anomalies detected in the U_{GEC} content and U_{MAS} content. Conversely, at the peripheries of uranium-rich geological bodies, local anomalies or high-value zones became apparent.

When uranium-rich geological bodies are buried at shallow depths, distinct peak anomalies in eU_{GGS} content can be observed directly above the ground, as well as in C_{Rn}, U_{GEC} content, and U_{MAS} content. Furthermore, the peaks in C_{Rn}, U_{GEC} content, and U_{MAS} content predominantly correspond to areas where the eU_{GGS} content slightly exceeds background levels.

After analyzing the spatial distribution characteristics of known sandstone-type uranium deposits in the Erlian Basin, such as the Hadatu and Barun deposits, as well as exploring different verification methods for prospecting indicators, combined with previous research on deep active uranium migration [5,17–20,24–29], we propose a new anomaly interpretation model in this paper. This model is based on the combination of GGS, C_{Rn}, GEC, and MAS measurement techniques, which are demonstrated in Figure 17. Therefore, in the process of interpreting the results of verifying AGS uranium anomalies and weak uranium anomalies, relevant attention should be paid to the areas exhibiting weakly elevated sections that correspond to low values of C_{Rn} and eU_{GGS} content. These areas may potentially indicate peak anomalies in U_{GEC} content or U_{MAS} content.

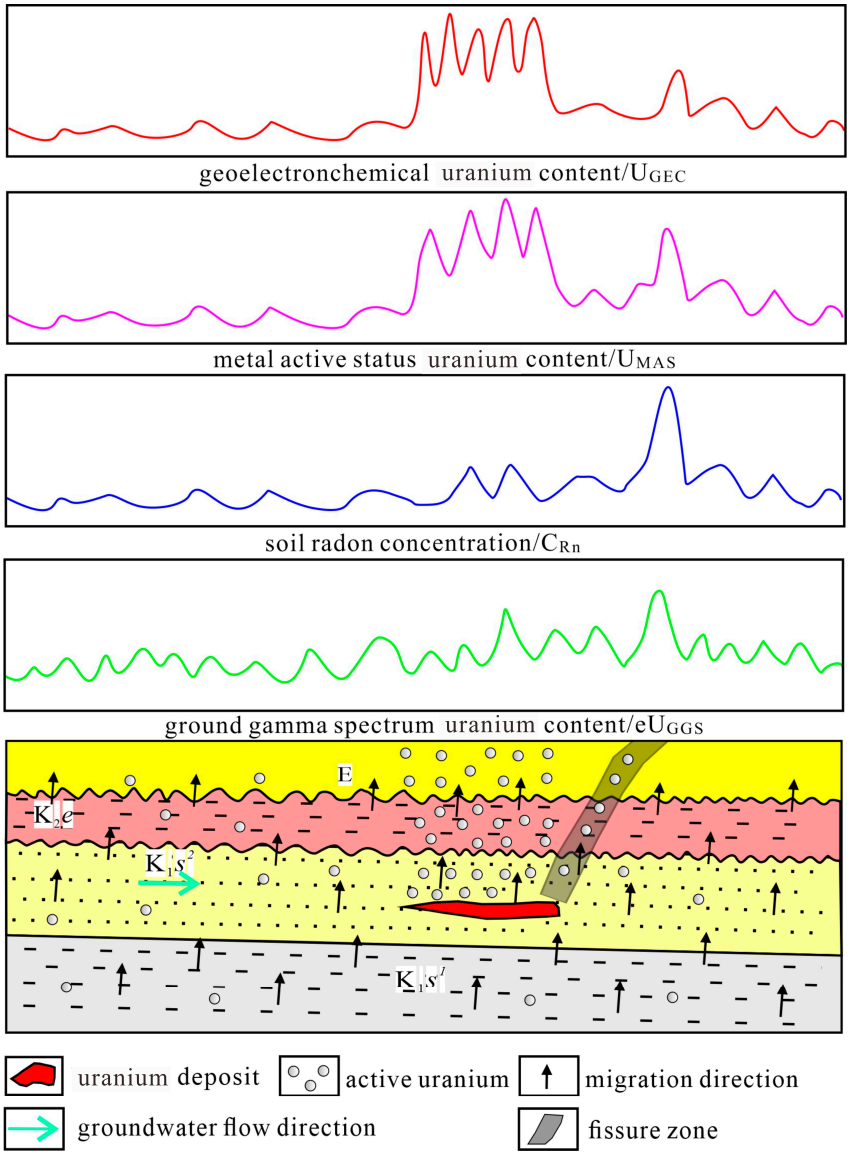


Figure 17. Schematic representation of an interpretive model for the combination anomaly of sandstone-type uranium deposits in the Erlian Basin.

5. Conclusions

This paper aims to study effective combination verification methods for AGS weak uranium anomalies in the coverage area of the Erlian Basin. This paper conducts multi-method verification research on known sandstone-type uranium deposits, AGS uranium anomalies, and weak information. The verification results of various methods in the four study areas were analyzed and studied. On this basis, the following conclusions were drawn:

1. According to the sandstone-type uranium metallogenic model in the Erlian Basin, when the buried depth of the uranium-rich geological body exceeds 100 m, the eUGGS content above these deep uranium bodies increases by (0.4–1.2) $\times 10^{-6}$ g/g compared to background areas, while the C_{Rn} levels at the edges of these bodies increase by more than 5000 Bq/m^3, which is 3–5 times higher than the regional average.
2. U_{GEC} and U_{MAS} content show sawtooth-like uranium peak anomalies in their profiles, and their peak-to-background ratio is greater than 5.
3. The correlations between C_{Rn}, eU_{GGS} content, U_{GEC} content, and U_{MAS} content are generally weak. However, there is a positive correlation at the top and edges of the enriched uranium geological body. The interpretation of anomalies should not merely analyze correlations but must consider the causes of anomalies based on comprehensive profile characteristics.

Author Contributions: Conceptualization, H.L. and N.W.; data curation, L.S., X.M., P.H., Z.S. and C.Y.; formal analysis, L.S.; funding acquisition, L.S. and N.W.; investigation, L.S., X.M., P.H., X.Z. and C.Y.; methodology, L.S. and H.L.; project administration, L.S. and N.W.; resources, L.S. and N.W.; supervision, N.W.; validation, L.S.; visualization, L.S.; writing—original draft, L.S.; writing—review and editing, L.S. and Z.S. All authors have read and agreed to the published version of the manuscript.

Funding: This research was supported by the National Natural Science Foundation of China [Grant number: U2067204], Airborne Survey and Remote Sensing of Nuclear Industry of China (202003) and China National Nuclear Corporation Geological Bureau (20194404).

Data Availability Statement: The datasets used and/or analyzed during the current study are available from the corresponding author on reasonable request.

Acknowledgments: Heartfelt thanks are extended to all the editors and reviewers for their valuable suggestions.

Conflicts of Interest: The authors declare no conflicts of interest.

References

1. Zhang, J.D. Innovation and development of metallogenic theory for sandstone-type uranium deposit in China. *Uranium Geol.* **2016**, *32*, 321–332.
2. Nie, F.J.; Yan, Z.B.; Feng, Z.B.; Li, M.G.; Xia, F.; Zhang, C.Y.; Wang, Y.G.; Yang, J.X.; Kang, S.H.; Shen, K. Genetic models and exploration implication of the paleochannel sandstone-type uranium deposits in the Erlian Basin, North China-A review and comparative study. *Ore Geol. Rev.* **2020**, *127*, 103821. [CrossRef]
3. Raghuwanshi, S.S. Airborne gamma-ray spectrometry in uranium exploration. *Adv. Space Res.* **1992**, *12*, 77–86. [CrossRef]
4. Karl, K.; Stephen, R. Innovative airborne geophysical strategies to assist the exploration of critical metal systems. *Geosystems Geoenvironment* **2025**, *4*, 100344.
5. Shi, L.C.; Zhang, X.; Yang, Y.Q.; Han, P.H.; Niu, J.J.; Lu, Y.Y.; Zhou, Z.J.; Shen, Z.X. Comprehensive geophysical and geochemical characteristics and research significance of Hadatu uranium deposit in Erlian Basin. *Geol. Explor.* **2022**, *58*, 274–285.
6. Hassan, S.M.; Youssef, M.A.; Gabr, S.S.; Sadek, M.F. Radioactive mineralization detection using remote sensing and airborne gamma-ray spectrometry at Wadi Al-Miyah area, Central Eastern Desert, Egypt. *Egypt. J. Remote Sens. Space Sci.* **2022**, *25*, 37–53. [CrossRef]

7. Shi, L.C.; Zhang, X.; Yang, Y.Q.; Han, P.H.; Niu, J.J. Airborne magnetic and radiometric characteristics and ore-prospecting significance of Hadatu Uranium deposit, Erlian Basin. *Geol. Rev.* **2021**, *67* (Suppl. S1), 187–188.
8. Shi, L.C.; Shen, Z.X.; Yu, C.; Yang, Y.Q.; Zhang, X.; Wang, Y.Y. Characteristics of airborne gamma spectrum and uranium migration of Barun uranium deposit, Erlian Basin. *Geol. Rev.* **2023**, *69* (Suppl. S1), 179–181.
9. Wu, Q.B.; Chen, C.; Yang, Y.Q.; Yu, X.; Gao, L.J.; Zhou, J.J.; Liu, W.S. Study of integrated geophysical characteristics of paleo-valley sandstone-type uranium deposits in the middle of the Erenhot basin. *Acta Geol. Sin.* **2021**, *95*, 2521–2536.
10. Li, B.H.; Wang, Y.; Wu, G.D.; Wang, D.S.; Zhu, W.F. Detecting method of concealed sandstone type uranium mineralization information in Songliao Basin. *Uranium Geol.* **2021**, *37*, 936–942.
11. Yan, D.Z.; Zhu, R.K.; Liu, W.H.; Liu, R.H.; Shou, H.; Cheng, X.; Cai, Y.F.; Lei, Z.F.; Deng, P.; Peng, Y. Metallogenic characteristics and models of sandstone-type uranium deposits in China. *Ore Geol. Rev.* **2024**, *166*, 105937. [CrossRef]
12. Liu, B. Study of Structure and Construction in Uranium-Bearing Paleo-Valley and Uranium Metallogenic Models in the Basaiqi Area, Erlian Basin. Master's Thesis, Jilin University, Changchun, China, 2018.
13. Wang, H. Research on the Soil Radon Data Processing Method and Abnormal Characteristics of Radon in a Sandstone-Type Uranium Deposit. Master's Thesis, Chengdu University of Technology, Chengdu, China, 2021.
14. Sajwan, R.S.; Joshi, V.; Ahamad, T.; Kumar, N.; Parmar, P.; Jindal, M.K. Assessment of radon transportation and uranium content in the tectonically active zone of Himalaya, India. *Sci. Total Environ.* **2024**, *926*, 171823. [CrossRef] [PubMed]
15. Grijalva-Rodríguez, T.; Valencia-Moreno, M.; Calmus, T.; Del Rio-Salas, R.; Balcázar-García, M. The El Horror uranium anomaly in northeastern Sonora, Mexico: Constraints from geochemical and mineralogical approaches. *J. S. Am. Earth Sci.* **2017**, *80*, 107–119. [CrossRef]
16. Shi, L.C.; Meng, X.B.; Lu, Y.Y.; Chen, Z.P.; Yang, Y.Q. Characteristics and prospecting significance of the HFU-14 airborne radioactive anomalies in the Alxa Zuoqi area, Inner Mongolia. *Geol. Explor.* **2019**, *55*, 999–1099.
17. Liu, W.S.; Li, B.H.; Shi, Q.P.; Jia, L.C.; Zhao, X.Q. Model and application of radon anomaly in soil of sandstone type uranium deposits in Erlian basin. *Geophys. Geochem. Explor.* **2015**, *39*, 234–239.
18. Yu, C.; Jia, B.L.; Shi, L.C.; Han, M.K.; Wang, N.P. Distribution of Radionuclides in the Surface Covering of the Barun Uranium Mining Area in Erlian Basin, Inner Mongolia. *Minerals* **2023**, *13*, 973. [CrossRef]
19. Luo, Q.B.; Yang, Y.X.; Zhang, Y.; Wu, X.M.; Zheng, Y.M.; Zhao, B.Y. Application and current status of geogas prospecting in concealed uranium deposits exploration. *Adv. Earth Sci.* **2018**, *33*, 75–84.
20. Guo, J.J.; Zhao, T.L.; Pan, W.; Wei, A.J.; Yin, Y.P.; Li, Z. Radon anomaly characteristics in the soil and uranium metallogenic prediction in Xianlaga depression of Erlian Basin. *Geol. Surv. China* **2024**, *11*, 25–31.
21. Zhang, B.M.; Lu, Y.X.; Wang, X.Q.; Zhou, J.; Li, H.W. Metal nanoparticles in soil: Indicators of concealed mineral deposits. *J. Geochem. Explor.* **2025**, *269*, 107633. [CrossRef]
22. Huang, J.L.; Chen, X.D.; Li, J.J.; Shan, C.T.; Hao, Y.Z. Prospecting middle and deeply buried sandstone-type uranium deposits beneath the Zhaosu Basin, Xinjiang by integrated geophysical methods. *Geol. Explor.* **2021**, *57*, 1099–1106.
23. Wang, X.Q.; Zhang, B.M.; Yao, W.S.; Sun, B.B. New evidences for transport mechanism and case histories of geochemical exploration through covers. *Earth Sci. J. China Univ. Geosci.* **2012**, *37*, 1126–1132.
24. Kang, H.; Chen, Y.L.; Li, D.P.; Zhao, J.X.; Cui, F.R.; Xu, Y.L. Deep-penetrating geochemistry for concealed sandstone-type uranium deposits: A case study of Hadatu uranium deposit in the Erenhot Basin, North China. *J. Geochem. Explor.* **2020**, *211*, 106464.
25. Zhang, B.M.; Wang, X.Q.; Zhou, J.; Han, Z.X.; Liu, W.S.; Liu, Q.Q.; Wang, W.; Li, R.H.; Zhang, B.Y.; Dou, B. Regional geochemical survey of concealed sandstone-type uranium deposits using fine-grained soil and groundwater in the Erlian basin, north-east China. *J. Geochem. Explor.* **2020**, *216*, 106573.
26. Liu, P.F.; Luo, X.R.; Wen, M.L.; Zhang, J.L.; Zheng, C.J.; Gao, W.; Ouyang, F. Geoelectrochemical anomaly prospecting for uranium deposits in southeastern China. *Appl. Geochem.* **2018**, *97*, 226–237. [CrossRef]
27. Ke, D.; Liu, H.J.; Hou, H.Q.; Wu, G.D.; Hao, W.J. Formation mechanism of electrochemical anomalies in interlayered oxidation type sandstone-hosted uranium deposit and its prospecting significance. *Acta Geol. Sin.* **2016**, *90*, 3545–3553.
28. Sun, B.B. Study on Formation Mechanism of Geoelectrochemical Anomaly and Standardization of Prospecting Technology. Ph.D. Thesis, China University of Geosciences (Beijing), Beijing, China, 2017.
29. Liu, H.J. Study on Electrochemical Extraction Technology of Sandstone-Type Uranium Deposits. Master's Thesis, Beijing Research Institute of Uranium Geology, Beijing, China, 2017.
30. Dou, B.; Zhang, B.M.; Wang, X.Q.; Liu, W.; Liu, Q.; Han, Z.; Zhou Jian, L.Y.; Liu Bin, Z.B.; Li, R. Experiment of prospecting sandstone-type uranium deposits by deep penetrating geochemistry in the Erlian Basin, Inner Mongolia. *Geol. Explor.* **2021**, *57*, 0380–0391.

31. Wang, G.H.; Yi, J.S. The application of mobile state uranium technique to the prospecting for sandstone type uranium deposits. *Geophys. Geochem. Explor.* **2000**, *24*, 358–362.
32. Yao, W.S. Leaching Mechanism and Conditions of Extractants on Mobile Forms of Elements in Soils. Ph.D. Thesis, Chinese Academy of Geological Sciences, Beijing, China, 2011.

Disclaimer/Publisher's Note: The statements, opinions and data contained in all publications are solely those of the individual author(s) and contributor(s) and not of MDPI and/or the editor(s). MDPI and/or the editor(s) disclaim responsibility for any injury to people or property resulting from any ideas, methods, instructions or products referred to in the content.